NASA TECHNICAL NOTE

NASA TN D-3859

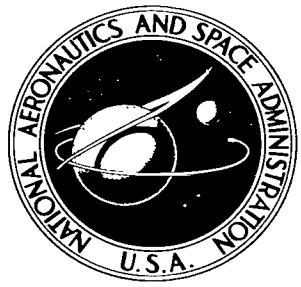

NASA TN D-3859

EFFECTS OF SHOCK-WAVE IMPINGEMENT ON THE HEAT TRANSFER ON A CYLINDRICAL LEADING EDGE

by Robert S. Hiers and William J. Loubsky

Ames Research Center
Moffett Field, Calif.

NATIONAL AERONAUTICS AND SPACE ADMINISTRATION • WASHINGTON, D. C. • FEBRUARY 1967

EFFECTS OF SHOCK-WAVE IMPINGEMENT ON THE HEAT TRANSFER ON A CYLINDRICAL LEADING EDGE

By Robert S. Hiers and William J. Loubsky

Ames Research Center
Moffett Field, Calif.

NATIONAL AERONAUTICS AND SPACE ADMINISTRATION

For sale by the Clearinghouse for Federal Scientific and Technical Information
Springfield, Virginia 22151 – Price $2.00

EFFECTS OF SHOCK-WAVE IMPINGEMENT ON THE HEAT TRANSFER ON A CYLINDRICAL LEADING EDGE

By Robert S. Hiers and William J. Loubsky
Ames Research Center

SUMMARY

This report describes an experimental study of the influence of shock-wave impingement on leading-edge heat-transfer and flow-field characteristics at a Mach number of 14. Heat-transfer measurements were obtained on the cylindrical leading edge of a blunted flat plate model at sweep angles of 0°, 22.5°, and 45°. The impinging shock waves were generated by deflecting a sharp flat plate attached at the root chord of the leading-edge model or were induced by boundary-layer separation on this "shock generator" flat plate. The angle of incidence of the shock generator was varied between 0° and 15°. The tests were conducted in the Ames 1-foot shock tunnel at a Reynolds number of 8000 based on the leading-edge diameter. A reservoir enthalpy of 10,500 J/g and a reservoir pressure of 290 atm were used for these tests.

Average heat-transfer rates as high as 2600 W/cm^2, more than 10 times the value with no shock impingement, were measured in small localized regions on the stagnation line of the unswept leading edge. The experimental results presented in this report suggest that this extreme interaction-induced effect on heat transfer is associated with the impingement of a vortex sheet or slip line (generated at the intersection of the bow shock wave and the impinging shock wave) onto the leading edge. Simplified boundary-layer calculations based on this vortex impingement model describe the general characteristics of the interaction-induced heat transfer to the unswept leading edge.

Heat-transfer rates 2-1/2 times the corresponding undisturbed value were measured over large spanwise segments of the stagnation line with leading edge swept 45° with respect to the free stream. At this sweep angle, however, the interaction-induced increase in heat transfer is not a localized result of the shock impingement similar to that found at zero sweep, since the vortex sheet associated with the intersecting shock waves does not impinge on the leading edge at this sweep angle. The leading-edge heat transfer in the interaction region can be adequately predicted at $\Lambda = 45°$ by applying infinite cylinder boundary-layer theory to the leading-edge flow field and utilizing conditions behind the impinging shock wave as the effective free stream. This result is in agreement with other studies of shock-wave impingement effects on highly swept leading edges.

Intermediate values of maximum heat transfer were obtained with the leading edge swept 22.5°. These values are apparently associated with the separation phenomena that occur on the shock-generator plate.

INTRODUCTION

The research program described in this report was designed to study the influence of shock-wave impingement on leading-edge heat transfer. Previous experiments (refs. 1 to 4, for example) have indicated that such interaction-induced effects on leading-edge heat transfer can be quite large in the region where the impinging shock wave intersects the leading-edge bow shock wave.

An examination of the literature indicates that several phenomena, depending upon the configuration under consideration, may influence this type of interaction-induced heat transfer. For example, Newlander (ref. 1) measured heat-transfer rates on an unswept leading edge up to three times the undisturbed value in a moderately supersonic stream, and attributed these phenomena to localized effects of the impinging shock wave. Several investigators later found that with the leading edge highly swept, the increased heat transfer was not a localized result of the shock-wave impingement itself. Bushnell (ref. 2) shows that the maximum heat transfer to a highly swept leading edge at a Mach number of 8 can be calculated by applying infinite cylinder boundary-layer theory, either laminar or turbulent, with local conditions obtained behind the impinging shock wave. Beckwith (ref. 3) found a similar result for a completely turbulent flow field at a free-stream Mach number of 4.15 and reasoned that Newlander's earlier results for an unswept leading edge might likewise be explained. Recently, however, Siler and Deskins (ref. 4) measured interaction-induced heat-transfer rates up to five times the corresponding undisturbed value on an unswept leading edge at a Mach number of 19, and it does not appear that infinite cylinder boundary-layer theory will explain their results. Francis (ref. 5) correlated, with only partial success, his heat-transfer measurements near shock-wave impingement by accounting for the spanwise entropy gradients produced by the intersection of the impinging and bow shock waves. In some of the investigations discussed here, additional regions of high heat transfer were observed in the interaction region and were attributed merely to "boundary-layer separation effects."

Two tentative conclusions can be drawn from the results of these experimental studies. First, the aerodynamic origin of the shock impingement effects on heat transfer is essentially known for highly swept leading edges. However, the aerodynamic origin of these effects for unswept leading edges or in the presence of boundary-layer separation on the shock-wave generator is generally not understood.

This investigation was conducted at a sufficiently low Reynolds number that the effects of extensive regions of separated flow on the shock generator could be studied under laminar flow conditions. The sweep angle of the leading edge was varied from 0° to 45° to investigate the aerodynamic mechanisms that give rise to interaction-induced heat transfer for various geometries.

SYMBOLS

b	model skin thickness, cm
c	heat capacity of model skin, J/g ^{o}K
d	diameter of leading-edge model, cm
h	specific enthalpy, J/g
M	Mach number
Pr	Prandtl number
$\dot{q}$	local heat-transfer rate per unit area, W/cm^2
Re	unit Reynolds number, cm^{-1}
R_{le}	leading-edge radius, cm
T	absolute temperature, ^{o}K
t	time, sec
V	velocity, m/sec
w	density of model skin, g/cm^3
x	spanwise distance along stagnation line measured from the location of maximum heat transfer, cm
y	spanwise distance along stagnation line measured from intersection of shock generator and leading edge, cm
δ	shock-generator angle of incidence or deflection angle, deg
Λ	leading-edge sweep angle, deg
μ	viscosity, Nsec/m^2

Subscripts

av	arithmetical average of wall and boundary-layer edge properties
d	diameter
o	reference value at stagnation line for appropriate sweep angle
t	total conditions in the shock tunnel reservoir

∞ free-stream conditions in test section

1-11 conditions for various flow regions defined in appendix A

FACILITY

This investigation was conducted in the 1-foot shock tunnel at Ames Research Center. A schematic diagram of the shock tunnel is shown in figure 1. Details of the design and operation of the shock tunnel are given in references 6 and 7. A nominal reservoir enthalpy of 10,500 J/g and a nominal reservoir pressure of 290 atm were used for these tests.

The test-section flow is generated by expanding the reservoir gas through a 10° half-angle nozzle into a 1-foot-square test section. Calibration measurements indicate the following state for the average test-section flow over the model:

$$M_{\infty} = 14$$

$$Re_{\infty,d} = 8000$$

$$U_{\infty} = 4270 \text{ m/sec}$$

$$T_{\infty} = 195^{\circ} \text{ K}$$

Nonequilibrium and conical nozzle effects, characteristics of the shock-tunnel flow, should not have much influence on the primarily convective phenomena of interest in this study. For example, the enthalpy in the frozen degrees of freedom in the test section is less than 10 percent of the total enthalpy.

MODEL

A photograph and sketch of the model used in this investigation are presented in figures 2 and 3, respectively. The shock generator is rotated relative to the leading-edge model through a series of internal gears to vary its angle of incidence, δ. The gap between the leading edge and shock generator was sealed before each test. The shock-generator plate was constructed from tool steel and had a sharp edge (thickness less than 0.05 mm). The internal structure of the leading-edge model is of rib and spar construction. The frame is covered with a 0.2-mm-thick sheet of type 302 stainless steel. The several slight imperfections in the geometry of the leading edge are insignificant for the purposes of this investigation.

The model was instrumented with chromel-constantan thermocouples. The nominal instrument locations are shown in figure 3. The relative locations of the thermocouples along the stagnation line were measured to within approximately 0.25 mm after installation. Number 40-gage thermocouple wires were used throughout except for monitor thermocouples where number 36-gage wires were used to insure long service. The thermocouple junctions were formed by

spot welding each wire of the junction to the back surface of the stainless-steel skin. The wires were laid flat on the skin less than 0.4 mm apart for spot welding. This unusually close spacing was used in spite of the associated wire conduction errors to improve spatial resolution in the heat-transfer measurements. The construction of the model is such that the effects of heat conduction from the skin to the internal supports are negligible.

TEST PROCEDURE

Heat-transfer data were obtained by the conventional transient heating technique. Steady flow is established in the shock tunnel nozzle approximately 1 msec after the reservoir is formed. Hence, the model, which is initially isothermal at room temperature, is exposed to the flow almost instantaneously as required by the technique. For this investigation, the free-stream flow was terminated with a valve located near the nozzle throat after approximately 20 msec. Longer test times could not be used for these tests because of the extremely high heat-transfer rates experienced by the model. The thermal response time or thermal lag of the model skin resulted in a delay of only 3 msec before the thermocouple instrumentation indicated the appropriate steady heating rate.

After suitable amplification, the thermocouple outputs were recorded on a high-speed oscillograph. Further details of the recording equipment are given in reference 8. The temperature-time history data were read every millisecond from the oscillograph trace and the resulting data, in digital form, were transferred to cards for machine computation. Heat-transfer data were machine reduced according to the usual calorimeter equation

$$\dot{q} = wbc \frac{dT}{dt}$$

One-dimensional lateral conduction effects are generally negligible in these data and are not considered in the data reduction. However, the two-dimensional (spanwise and normal directions) conduction effect must be considered in the analysis of data obtained in certain localized regions of rapidly varying heat transfer. This effect is discussed further under Results and Discussion and in appendix B. It is estimated that the total uncertainty in these heat-transfer data is less than ±20 percent.

Still and high-speed motion pictures of the self-luminous flow around the model were obtained during most tests. In addition, schlieren photographs were obtained of the flow over the model. Oil-flow results of the surface flow on the shock generator and leading-edge model were also obtained. Tunnel starting and shut-down times are believed to have a negligible influence on the oil-flow results. Heating rates on the model were so great that small regions of the leading-edge surface were oxidized during some tests. The resulting burn-mark patterns were used to determine the location of maximums in the local heat transfer in much the same manner that temperature-sensitive paint is used. It is estimated that the location of peak heat transfer was determined to an accuracy of 0.2 mm by this technique.

RESULTS AND DISCUSSION

The results of this study are presented as follows: First, flow visualization data are presented to define the gross features of the flow field in the interaction region formed by the intersection of the impinging and leading edge bow waves. Then, the measured heat-transfer data are presented and correlated with these flow-field results to establish tentatively the origin of the observed interaction-induced effects on heat transfer. A mathematical flow model, based on the flow visualization results and developed in appendix A, is used to estimate heating rates in the interaction region. Finally, the flow-field data, heat-transfer data, and the calculated heat transfer are correlated to indicate the origin of the important characteristics observed in the heat-transfer data.

Flow Visualization Results

Self-luminous flow-field results.- Typical luminous flow-field results obtained on the unswept leading edge with the shock generator at 10° angle of incidence are shown in figure 4. A self-luminous photograph is presented in figure 4(a), and the important features are shown schematically in figure 4(b).

The distinct demarcation line between the luminous and nonluminous regions over the afterbody of the cylindrically blunted flat plate is associated with the shock wave originating at the leading edge of the shock generator. This conclusion agrees with the results of figure 4(b) where excellent correlation between the locations of the calculated shock wave and the demarcation line is observed. The boundary-layer interaction theory and the shock-expansion theory presented by Hayes and Probstein (ref. 9) are used to simultaneously determine the displacement thickness of the boundary layer on the shock generator and the location of generated shock wave. The schlieren results presented in the next section also confirm that this demarcation line coincides with the generated shock wave.

The region of intense luminosity on the shock generator immediately upstream of the cylindrical leading edge is associated with an extensive area of separated and reverse flow. It is not possible to establish with certainty whether this luminosity represents the shock wave induced by the boundary-layer separation or the reverse flow region associated with separation. In either event, the separation shock wave lies near the luminous region because the local Mach number is high. The estimated location of the separation shock wave, in relation to the luminous regions, is shown schematically in figure 4(b). The origin of the separation shock wave is believed to coincide with burn marks (to be described later) on the shock-generator plate.

The luminous photograph results presented in figure 4 are generally typical of those obtained for the unswept leading edge ($\Lambda = 0^{\circ}$) throughout the range of shock-generator angles from 0° to 15°. At $\delta = 0^{\circ}$ the luminous

region associated with boundary-layer separation on the shock generator nearly coalesces with the generated shock wave, indicating that the separation-induced shock wave probably coalesces with the generated shock wave. Knox (ref. 10) presents schlieren results that show the separation and generated shock waves coalescing to a single shock wave of greater strength under similar conditions. However, for these test conditions, the agreement between the luminous flow-field results and the above-mentioned shock-wave calculations indicates that the strength of the generated shock wave is not significantly increased when it coalesces with the separation-induced shock wave. As the shock-generator deflection angle is increased, this luminous region decreases, indicating that the separation-induced and the generated shock waves tend to diverge.

As the sweep angle is increased to 22.5° and 45° the luminous region associated with boundary-layer separation on the shock generator becomes small and then essentially vanishes at all shock-generator positions indicating that very little boundary-layer separation occurs at these sweep angles.

Note that the bow shock wave is not parallel to the leading edge just outboard of the shock-wave intersection region. As a result, the flow in this region has a velocity component in the spanwise direction as it approaches the leading edge. The schlieren results presented in the next section also indicate that the bow shock wave is curved in this region.

Schlieren results.- Figure 5 is a schlieren photograph of the flow on the unswept leading edge with the shock generator deflected 15°. The details of the shock-wave patterns in the interaction region cannot be determined from these results. However, the general shape of the cylindrical bow shock wave and the generated shock wave can be determined from the original schlieren photographs. The location of the generated shock wave is in good agreement with the corresponding shock-wave calculations and with the luminous photograph results of figure 4. Notice, from this figure, that the cylindrical bow shock wave becomes two-dimensional only at relatively large spanwise distances outboard of the interaction region. The effect of the "yawed" bow shock wave outboard of the interaction region is shown in the oil-flow results in the next section.

Although schlieren results were obtained only for the configuration presented in figure 5 ($\delta = 15^\circ$, $\Lambda = 0^\circ$), these results are believed typical of the shock-wave pattern that exists at $\Lambda = 0^\circ$ for all shock-generator deflection angles.

Surface oil-flow results.- Typical oil-flow results for the surface flow on the shock generator are presented in figure 6 for $\Lambda = 0^\circ$, $\delta = 10^\circ$. Figure 6(a) shows results obtained by two different oil deposition techniques. One technique consists of uniformly covering the model surface with a thin coating of low viscosity oil that contains powdered graphite. The other technique consists simply of placing small drops of high viscosity grease at selected locations. Figure 6(b) is a composite sketch of the flow patterns

obtained from these results. The boundary-layer separation and reverse flow on the shock generator are illustrated in these results. Notice that the reverse flow is initially radial and becomes essentially circumferential at large distances from the leading-edge, shock-generator junction.

The extensive lateral flow on the shock-generator plate is primarily a result of the boundary-layer separation and reverse flow phenomena on the shock-generator plate. The inconsequential effects of the finite span of the plate are seen in the region of undisturbed flow on the shock-generator plate upstream of the boundary-layer separation.

In contrast to the result in figure 6, the data obtained with the leading-edge model swept show only small, if any, regions of separated or reverse flow on the shock generator at $\Lambda = 22.5^{\circ}$, and essentially no separation at $\Lambda = 45^{\circ}$. Recall that this result is in agreement with the luminous flow-field data.

A photograph of an oil-flow test of the leading edge is presented in figure 7 for $\delta = 15^{\circ}$ and $\Lambda = 0^{\circ}$. This figure shows that the flow near the stagnation line of the leading edge has a predominantly spanwise component of flow in the interaction region. A region of apparently undisturbed cylindrical flow exists near the outboard tip of the leading-edge model. Edge effects extend no more than approximately one leading-edge diameter inboard from the tip. The flow just inboard of the undisturbed cylinder flow appears to be characteristic of the flow on a swept leading edge. As previously mentioned, the schlieren photograph of the bow shock wave (fig. 5) indicates that the leading edge experiences a slightly yawed local flow in this region. The two regions of oil accumulation on the leading edge indicate regions of separated flow. The flow between these accumulations has both an outboard and inboard spanwise component separated by an apparent parting line. Typically, most of the oil in the streak filaments at the parting line was removed, as seen in figure 7, because of the combined effects of high local surface shear near the parting line and high local heating that decreases the viscosity of the oil.

Notice that in figure 7 two locations on the stagnation line are labeled shock-wave impingement. These positions are determined from the surface burn mark results presented in the next section and correspond to regions of very intense surface heat transfer. The relationship between these burn marks and the impinging shock waves will be described later. Because of the relatively poor spatial resolution of the oil-flow methods, the local details of the surface flow associated with these burn marks cannot be seen.

At lower deflection angles (δ) only one shock wave impinges at the leading edge; a single burn mark is produced instead of the two described with respect to figure 7. A schematic interpretation of the surface flow on the leading-edge model and of the external flow ahead of the model is shown in figure 8 for a case with only one impinging shock wave. The results of figure 7 provide the primary experimental guide from which the diagram in figure 8 is derived (although these two cases differ in detail as just described). Although figure 8 is a very simplified representation of the flow field, it does qualitatively suggest the origin of many of the results found

on the oil-flow photographs. The two regions of separated flow on the leading edge in figure 7 can be rationalized in terms of this flow diagram. The correlations, to be discussed in the heat-transfer results, indicate there is a parting line originating where a vortex sheet or slip line impinges on the leading edge. This vortex sheet is, of course, the usual discontinuity associated with the intersection of two shock waves of opposite family. This parting line is an area of extremely intense heat transfer. Portions of the flow over the leading edge can be treated as predominantly two-dimensional for simplicity, as indicated by figure 8, but there are locations where three-dimensionality must be considered since the flow must obey the basic mass conservation principles. One such location is near the reverse flow immediately below the point marked "oil accumulation" in figure 8.

The region of reverse flow on the shock generator (figs. 6, 7, and 8) is not the usual recirculating type flow associated with two-dimensional separation at a compression corner. The streamline pattern in the neighborhood of a typical two-dimensional separation (shown in fig. 9 for comparison with the present results) is not influenced by an impinging shock wave. The dividing streamline in this conventional separation phenomena lies in the shear layer as shown in figure 9. However, the flow-field diagram shown in figure 8 indicates that the dividing streamline, at the surface of the leading-edge model, is the "vortex sheet." For these conditions, the shear layer that forms as a result of boundary-layer separation on the shock generator does not "wet" the leading-edge model. Instead, the flow along the leading edge appears to be fluid turned inboard by the shock waves. This fluid then flows out radially along the shock-generator plate (fig. 6) and finally flows circumferentially along the plate and out of the interaction region. The importance of three-dimensional effects in the separation pattern on a cylinder with an impinging shock wave were previously pointed out by Halprin (ref. 11).

Surface "burn-mark" results. - Typical "burn-mark" results are presented in figure 10. The results in figure 10(a) are representative of the best quality burn-mark data obtained on the shock-generator plate. The results in figure 10(b) are representative of the best quality burn-mark data obtained on the leading edge. These data are in accord with the flow-field data presented in figures 4 to 7. In particular, the separation line on the shock generator is a region of high local heat transfer, as evidenced by a semicircular burn mark several leading-edge radii upstream of the cylindrical leading edge (fig. 10(a)). Observe that the "stagnation line" on the shock-generator plate, indicated in the oil-flow results of figure 6, is also a region of high heat transfer.

For the purposes of this investigation, the burn marks on the cylindrical leading edge are of primary interest. For the particular configuration presented in figure 10(b), two definite burn marks occur near the spanwise location for the intersection of the generated and bow shock waves. This figure is presented in color to retain all possible resolution and detail. For the analysis presented later it is extremely important to know that two burn marks occurred. The thermocouple instrumentation did not always detect both burn marks because of the extreme sharpness of the heat-transfer peaks. Two burn marks are also obtained on the configuration with $\Lambda = 0^{\circ}$ and $\delta = 10^{\circ}$

although they are slightly closer together. The burn marks are partially visible in the data of figure 10(a) although they are somewhat obscured by a coating on the model surface and by the photograph being black and white. For smaller angles of incidence of the generator plate only one burn mark is found on the leading edge. This burn mark corresponds to the "parting line" of figure 8 and hence to the impingement of a vortex sheet onto the leading edge. It will be shown that two burn marks appear at $\delta = 10^{\circ}$ and $\delta = 15^{\circ}$ because the generated and separation shock wave form separate vortex sheets that intersect the leading edge.

In general, the burn marks associated with the impinging shock waves indicate that the regions of peak heating are very localized in spanwise extent and that the heat flux itself is quite intense. A comparison of the features of the burn marks indicates that the local heat-transfer rates associated with these burn marks are of similar magnitude for all shock-generator deflection angles. The spanwise position of these burn marks will be used in a later section to determine the location of the parting line and the theoretical maximum heat transfer.

In addition to the burn marks associated with the impinging shock waves, a less intense burn mark occurs on the leading-edge model adjacent to the outboard separation mentioned previously in the discussion of figure 8. This burn mark is barely visible in figure 10(b) since this region has only moderately high heat transfer.

These burn mark results, as well as the other flow visualization data presented in this section, are correlated with heat-transfer measurements in the next section.

Heat-Transfer Results

Stagnation line heat-transfer data, $\Lambda = 0^{\circ}$.- Heat-transfer rates measured on the stagnation line of the unswept leading-edge model are presented in figure 11 for shock-generator deflection angles of 0°, 2.5°, 5°, 10°, and 15°. The data are normalized with the stagnation point heat-transfer rate calculated by the method of Fay and Riddell (ref. 12) for equilibrium flow at the free-stream conditions. The normalized heat-transfer rates (circular symbols) are plotted in figure 11 as a function of spanwise distance along the stagnation line. The calculated and measured intersection of the generated shock wave with the leading-edge bow shock wave, shown in figure 11 as a triangular symbol, are essentially coincident. The location of heat-transfer peaks, determined from burn markings, is indicated by the spanwise position of the square symbols; the maximum heat transfer at that location will be discussed in the next section along with the curve marked "calculated heat transfer." The spanwise position of the separation line noted on figure 7 is also indicated in figure 11(e). The flagged symbols in figures 11(a) and 11(d) were data, measured 15° from the geometrical stagnation line extrapolated to the stagnation line along a line that coincides with the burn mark obtained on each configuration. The magnitude of the data was not altered during the extrapolation. Notice that there is a slight displacement between the data

obtained at the stagnation line and the corresponding data at the 15° chord position since the burn mark is not perpendicular to the leading edge. The additional data points in figure 11(d) were obtained by shifting the shock-generator plate in a spanwise direction.

The significant disturbance-induced effect on heat transfer generally occurs inboard of $y = 2.0$ cm for each configuration shown in figure 11. At a spanwise distance of $y = 2.5$ cm, the effects of the interaction are no longer felt in the stagnation-line heat transfer. Good agreement is obtained between the measured heat transfer and the equilibrium theory of Fay and Riddell at this location. The leading edge experiences a yawed local flow in this region, according to the oil-flow results of figure 7; however (since stagnation-line heat transfer varies approximately as the cosine of the yaw angle), this effect is negligible for the small values of local yaw angle shown in figure 8.

Since the high peak heating rates are very localized, the location of heat-transfer maximum coincided with a thermocouple location for only one of the configurations tested. The heating rate at that location, shown in figure 11(b) at $y \approx 1.45$ cm, is more than 10 times the corresponding undisturbed heating level. A thermocouple location almost coincided with a heat-transfer maximum for the configuration shown in figure 11(d). The measured heat transfer at that position changed substantially with time during the test because of the slight movement of the maximum. The double valued point in figure 11(d) at $y \cong 1.2$ cm represents the extremes in heat transfer measured during the test. It is estimated that a movement of the location of peak heating of the order of 0.2 mm could cause the observed variation.

The measured peak heat transfer is, in effect, an average since the data in figure 11 indicate that the local heating rate varies substantially across the face of the sensible surface area on which the measurement was made. The skin thickness determines the spanwise extent of the averaging for the type of instrumentation used in these tests. (The preceding discussion assumes that the separation of the thermocouple wires on the inner surface of the skin is of the same order or less than the skin thickness as was the case for the results presented here.)

At this point it is obvious how critical the burn-mark data are in the interpretation of the heat-transfer results. For example, burn marks of approximately equal intensity were obtained for $\Lambda = 0^{\circ}$, $\delta = 2.5^{\circ}$, and $\Lambda = 0^{\circ}$, $\delta = 5^{\circ}$. However, the corresponding heat-transfer data (figs. 11(b) and 11(c)) show the high peak for one case but not for the other case because of the sharpness of the peaks.

It is apparent in figure 11 that excellent correlation is obtained between the intersection of the generated shock wave with the leading-edge bow shock wave and the location of the outermost peak in heat transfer. This correlation indicates that the peak is directly associated with the impingement of the generated shock wave onto the cylindrical bow shock wave. It is also observed that the inboard peak (when two peaks exist) moves inboard as the deflection angle, δ, is increased. The position of the

inboard peak correlates with the estimated location of the separation shock wave. This suggests that the inboard peak is related to the impingement of the separation shock wave onto an imbedded bow shock wave.

Stagnation-line heat-transfer analysis, $\Lambda = 0^{\circ}$.- According to simple two-dimensional shock-wave theory, the generated shock wave would not be transmitted through the bow shock wave to the leading edge; a vortex sheet, formed at the intersection of these two shock waves, would intersect the leading edge as indicated in figure 8. A theoretical analysis of the flow and heat transfer near the heating maximum is developed in appendix A based on the assumption that the impingement of this vortex sheet controls the heat transfer near the peak. These calculations predict the peak heat transfer, associated with the generated shock wave, shown by the unfilled square symbols in figure 11. Recall that the spanwise position of the square symbols is taken to be the measured location of the maximum heat transfer as determined from burn-mark results. The theoretical distribution of heat transfer in the neighborhood of these peaks is also shown in figure 11 for each configuration.

According to the simplified analysis presented in appendix A, the local heat-transfer maximum goes to infinity. However, the thermal averaging due to finite skin thickness results in a finite maximum as explained in appendix B.

The measured and theoretical peak heat transfer (2600 W/cm^2) are in good agreement in figure 11(b), the only configuration for which the location of the maximum heat transfer coincided with a thermocouple location. The measured and theoretical (outboard) peak heat transfer are in fair agreement in figure 11(d) where a thermocouple location was near but not coincident with the heating maximum.

The experimental and theoretical distribution of heat transfer are in reasonable agreement near the heat-transfer peak for $\delta = 0^{\circ}$ and $\delta = 2.5^{\circ}$ (figs. 11(a) and 11(b)). At some distance from the peak, local conditions depart appreciably from the two-dimensional constant-pressure flow assumed in the theory; hence, the disagreement between theory and experiment at substantial distances from the peak is expected. The above results indicate that the separation shock wave does not produce a separate influence on the local heat transfer just inboard of the peaks for $\delta = 0^{\circ}$ and $\delta = 2.5^{\circ}$ in agreement with burn-mark results. This is anticipated because the separation shock wave apparently coalesces with the generated shock wave at these conditions, as mentioned previously.

However, the separation shock wave does not coalesce with the generated shock wave at larger shock-generator deflection angles. Hence, the separation shock wave is expected to cause a separate disturbance in the leading-edge heat transfer at the larger deflection angles. The significant discrepancy between the measured and theoretical heat transfer at $y \cong 1.1$ cm for $\delta = 5^{\circ}$ (fig. 11(c)) is believed to result from the effects of the separation shock wave. The effect of the separation shock wave on leading-edge heat transfer becomes very pronounced as the shock-generator deflection angle is further increased to $\delta = 10^{\circ}$ and $\delta = 15^{\circ}$. Notice that at these deflection angles there is a definite inboard peak in heat transfer indicated in figures 11(d)

and 11(e) and verified by the burn-mark data. This inboard peak can probably be associated with the impingement of the separation shock wave onto an embedded bow shock wave. The theoretical method developed in appendix B cannot be applied numerically to the inboard peak in heat transfer since the appropriate inviscid conditions are not known.

The vortex impingement model, based on the experimental flow field results presented here, qualitatively accounts for most of the phenomena observed in this study while the simplified heat-transfer calculations based on this flow-field model provide interesting, although not conclusive, quantitative agreement with the heat-transfer data. Thus, it appears that the mechanism of vortex impingement, proposed in the appendices to explain interaction induced effects or heat transfer on unswept leading edge, is useful. However, the details of the calculation procedures presented in the appendix considerably simplify the aerodynamic processes and contain certain arbitrary, though reasonable, assumptions in order to yield analytical results.

Extreme heat-transfer maximums similar to those found in this study have been observed in several other investigations. However, in those studies by Siler and Deskins (ref. 4) and Ray and Palko (ref. 13), for example, no specific explanation of the phenomena is given. In this regard, it is observed that, in addition to being hampered by sparsely located heat gages, the instrumentation used in these studies does not appear capable of the spatial resolution required to measure the details of local heating distributions such as found in the present study.

The heat-transfer distribution observed on the stagnation line of the unswept leading edge cannot be predicted by applying infinite cylinder boundary-layer theory locally to the interaction flow field over the cylindrical leading edge. Several investigators, including Jones (ref. 14), have found that this technique describes the stagnation-line flow and heat transfer on swept leading edges provided shock-generator conditions are used as an effective free stream. Beckwith (ref. 3) speculated that this technique might be applicable to unswept leading edges as well. However, it is now apparent that this method does not account for localized effects observed in the present study on unswept leading edges. Francis (ref. 5) attempted to account for the localized influence of shock-wave impingement in an essentially two-dimensional cylinder type flow field by introducing the effect of spanwise entropy gradients (formed as a result of the shock-wave intersection) in the local inviscid flow approaching the leading edge. Unfortunately, Francis did not show local spanwise heat-transfer distributions or discuss his instrumentation thoroughly (skin thickness, gage spacing, etc.). However, it now appears from a consideration of the oil-flow results of the present study that none of the "quasi-two-dimensional" cylinder flow models are consistent with the flow fields observed in this study.

Stagnation-line heat-transfer results, $\Lambda = 22.5^{\circ}$.- Heat-transfer rates measured on the stagnation line of the leading edge at a sweep angle of $\Lambda = 22.5^{\circ}$ are presented in figure 12 for shock generator deflection angles of 0° and 10°. These data are normalized with the theoretical equilibrium heat transfer to a swept stagnation line in the absence of an impinging shock wave.

A simple cosine variation of stagnation-line heating with sweep angle was used with the theory of Fay and Riddell to calculate the reference value of heat transfer. In figure 12 the flagged symbols represent stagnation-line heat-transfer results that were obtained by extrapolating chordwise heat data perpendicular to the stagnation line.

The disturbance-induced effects on heat transfer do not extend beyond approximately $y = 2.5$ cm, where good agreement is obtained between the measured and the reference heat transfer $\dot{q}_o$. In this regard the disturbance-induced effects on heat transfer extend over a larger spanwise distance for $\Lambda = 22.5^\circ$ than for $\Lambda = 0^\circ$.

An obvious difference in these data and the corresponding data obtained on the unswept leading edge is the absence of a heat-transfer peak associated with the intersection of the generated shock wave and the bow shock wave with the leading edge swept 22.5° (figs. 12(a) and 12(b)). This is confirmed by the absence of burn marks in this region. The vortex sheet formed at the shock-wave intersection may be swept in an outboard spanwise direction when the leading edge is swept as a result of the spanwise component of flow between the bow shock wave and the leading edge.

A heat-transfer maximum, inboard of the impingement of the generated shock wave, is shown in figure 12. The maximum heat transfer measured at this sweep angle (although not necessarily the actual peak value) is approximately seven times the corresponding undisturbed level (fig. 12(b)).

At least two descriptions of the flow field could explain the single heat-transfer maximum observed at $\Lambda = 22.5^\circ$. First, the maximum may be the result of the impingement of a separation shock wave onto an imbedded bow shock wave. The maximum would then be analogous to the inboard peak heat transfer observed at $\Lambda = 0^\circ$. Alternatively, since the model simulates a steep compression corner at $\Lambda = 22.5^\circ$, the single maximum may be associated with the conventional reattachment heat transfer found near compression corners such as shown in figure 9. The data obtained during this study do not permit one to choose with certainty between these alternative descriptions of the flow field. In any event, the disturbance-induced effects on heat transfer appear to be associated with the separation phenomena on the shock-generator plate.

Stagnation-line heat-transfer results, $\Lambda = 45^\circ$.- Heat-transfer rates measured on the stagnation line of the leading edge at a sweep angle of $\Lambda = 45^\circ$ are presented in figure 13 for shock-generator deflection angles of 0° and 10°. These data are normalized as described in the last section.

The disturbance-induced effects on heat transfer extend the entire span of the instrumentation at this sweep angle. In contrast to the results presented for $\Lambda = 0^\circ$ and $\Lambda = 22.5^\circ$, no region of very intense peak heating is associated with either the generated or a separation shock wave. Instead, only a relatively moderate increase over the undisturbed level of heat transfer occurs over a wide region of the span. In addition, the local heat transfer is considerably lower than its corresponding undisturbed value over a

significant portion of the span outboard of the generated shock impingement. The maximum heat transfer measured on the stagnation line is approximately 2-1/2 times as large as the undisturbed heating level at this sweep angle for deflection angles of 0° and 10°. Notice in figure 13 that the location of maximum heat transfer at $\delta = 0^\circ$ is considerably outboard of the maximum at $\delta = 10^\circ$. This appears to be related to the movement of the generated shock wave.

Since essentially no separation was detected on the shock generator at this sweep angle, the absence of intense peaks is then consistent with the flow models suggested for $\Lambda = 22.5^\circ$.

The heat-transfer distribution near the maximum heating in figure 13(b) is relatively flat. This suggests that an approximately two-dimensional flow field exists in this region. Hence, the technique proposed in reference 2 can be applied to estimate the heat transfer in this region. The heat transfer is calculated by assuming a two-dimensional cylinder type flow over the leading edge with inviscid conditions on the shock generator as an effective free stream. Fair agreement is obtained between this calculation and the experimental results in figure 13(b). The local conditions outside the boundary layer used in the calculation are determined by assuming that the flow over the shock generator passes through only one imbedded shock wave parallel to the leading edge before reaching the stagnation line. Actually, multiple compressions may exist in this region. The agreement between theory and experiment would improve if these compressions were considered since the local pressure would thereby be raised. Hence, the results of the present investigation are in reasonable agreement with references 2 and 3 where, for large sweep angles, no direct localized effect of shock-wave impingement on leading-edge heat transfer was found in the absence of separation on the shock generator. The technique of reference 2 was not applied to the data in figure 13(a) because there is no significant spanwise region of the leading edge with essentially constant heat transfer which, of course, implies that the flow is not approximately two-dimensional.

CONCLUDING REMARKS

Order of magnitude increases in the stagnation-line heat transfer were observed in localized regions of the unswept leading edge as a result of shock wave impingement. These intense maximums in the heat-transfer rates, as high as 2600 W/cm^2, are average values measured on a small spanwise region of the stagnation line over which the local heat-transfer rate changes substantially. These interaction-induced effects on heat transfer apparently arise where the vortex sheet formed by the intersection of the impinging shock and the bow shock waves strikes the leading edge. The local flow field in the interaction region of the unswept leading edge is not two-dimensional cylindrical flow.

The effects of shock-wave impingement on maximum leading-edge heat-transfer rates decrease as sweep angle increases. Maximum values of interaction-induced heat-transfer rates of approximately seven times the

corresponding undisturbed value were observed on the leading edge at a sweep angle of 22.5°. The interaction-induced effects at this sweep angle appear to result from the boundary-layer separation phenomena on the shock-wave generator. The generated shock wave itself apparently produces no separate localized disturbance in this case, such as observed on the unswept leading edge. The heat-transfer rates at a sweep angle of 45° can be predicted adequately by applying two-dimensional boundary-layer theory to an equivalent swept-cylinder flow field and using conditions behind the generated shock wave as the effective free stream.

Ames Research Center
National Aeronautics and Space Administration
Moffett Field, Calif., Nov. 3, 1966
126-13-03-02-00

APPENDIX A

FLOW MODEL

A simplified model for the flow near the intersection of a bow shock wave and an impinging shock wave is used to calculate heat-transfer rates to the cylindrical leading edge that generates the bow shock wave. The impingement of the vortex sheet emanating from this shock-wave intersection onto the leading edge is assumed to control the maximum heat transfer to the leading edge. The theoretical heat transfer due to the impingement of this vortex is calculated by means of a simplified boundary-layer analysis in conjunction with appropriate inviscid conditions.

The general features of the flow field in the interaction region (see fig. 8 of the text) are shown in sketch (a). Recall that the flow is

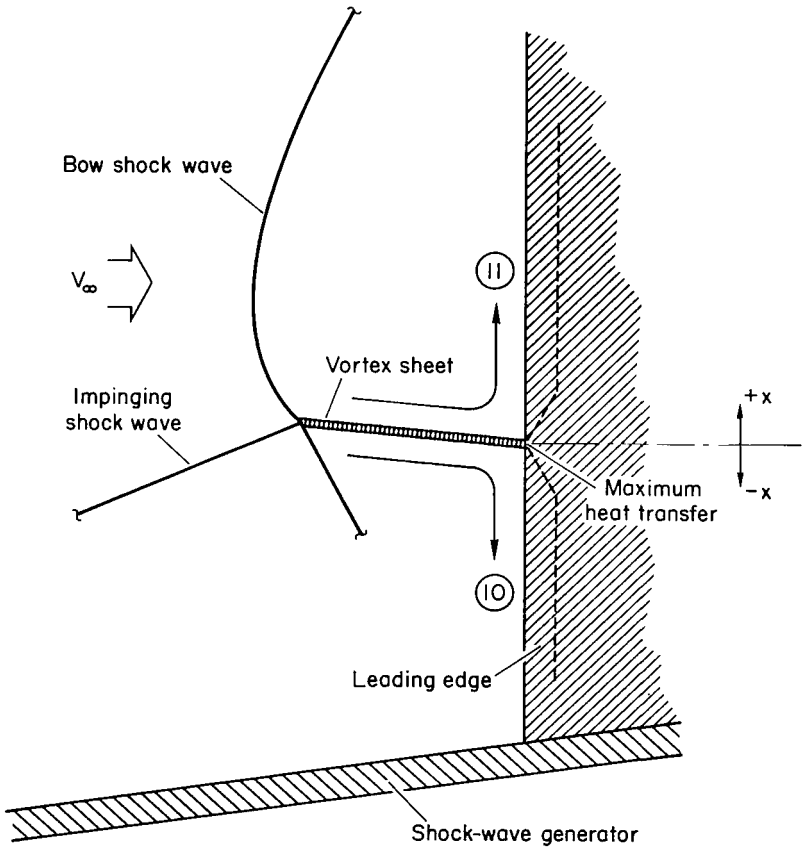

Sketch (a)

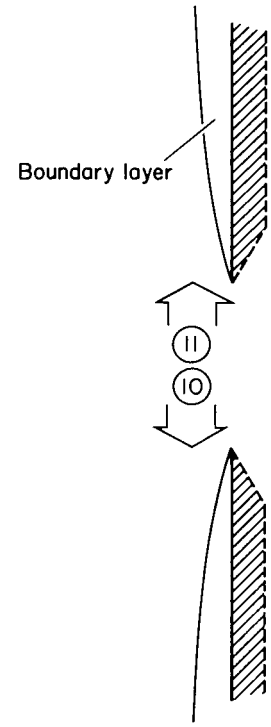

Sketch (b)

predominantly spanwise in the neighborhood of the parting line as indicated by the oil-flow results in the text. The simplest flow field model for the surface flow near the parting line consistent with these results is that of a flat plate where the parting line is considered to be the leading edge. For this analysis the flow is therefore postulated to behave in this simplified manner. Thus, the parting line is treated as a flow attachment line. The boundary layer is then assumed to originate with zero thickness at the parting line and is assumed to develop in the spanwise direction under the influence of a flat-plate type of inviscid flow. Chung and Viegas (ref. 15) also assumed the boundary layer to originate with zero thickness at the flow attachment line for a somewhat similar impinging flow. Hence, for mathematical analysis, the flow near the vortex impingement is replaced by the model shown in sketch (b), where the streams labeled 10 and 11 are considered to be uniform, parallel flat-plate type flows originating at the parting line. The relationship between this assumed mathematical model and the physical flow is indicated by the dashed lines in sketch (a). This model provides one of the simplest mathematical and physical approximation that is consistent with the observed flow-field characteristics described in the text.

The surface heating rate for the flow model of sketch (a) is calculated simply using the constant property Blasius solution given by Schlichting in reference 16. The result for region 10 of sketches (a) and (b), written in terms of average boundary-layer properties, is:

$$\dot{q}_{10} = 0.332 \frac{\mu_{av}}{Pr_{av}^{2/3}} \frac{(Re_{10})^{1/2}}{x^{1/2}} h_t \qquad (A1)$$

This expression is written in terms of enthalpy and for the cold-wall approximation, since a high-temperature partially dissociated gas is under consideration. An expression similar to equation (A1) can be written for region 11.

To evaluate equation (A1), the appropriate inviscid conditions in regions 10 and 11 of sketch (b) must be found. Ideally, one would determine the necessary parameters in terms of the known free-stream properties using shock-wave angles, etc., obtained from schlieren or other optical results. However, since these optical data were not available for this study, it was necessary to calculate the appropriate inviscid conditions using the flow-field approximation shown in sketch (c).

The flow in the interaction region is considered to behave as a perfect gas since the chemical and vibrational energy exchange processes are essentially frozen for the flow. The strength of the generated shock wave at intersection A is found from the calculations indicated in the text. The conditions downstream of intersection A are determined by adjusting the strengths of the bow shock wave and the reflected shock wave so that the pressures and flow directions in regions 2 and 4 are approximately equal. The reflected shock wave at intersection A is assumed to propagate with constant strength to intersection B. The conditions downstream of intersection B are then found in a manner similar to that for intersection A. Depending upon the particular flow field being considered, an additional shock wave (or

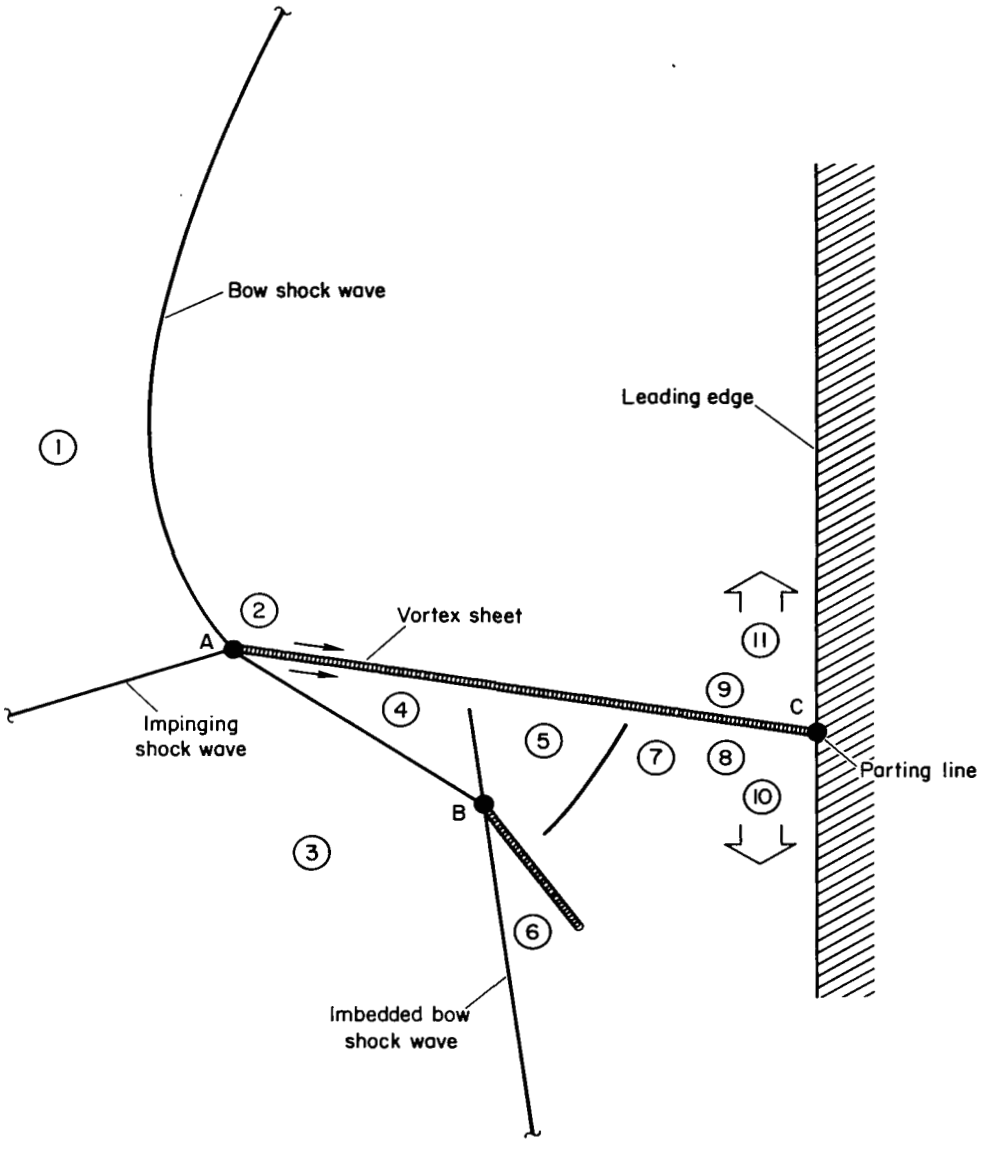

Sketch (c)

expansion fan) can exist at intersections A and B. However, these additional waves are usually weak and are neglected for simplicity. It is assumed that the flow in region 5 is decelerated by the normal shock wave shown in sketch (c). It is also assumed that the inviscid conditions in regions 9 and 11 as well as in regions 8 and 10 are equal. The previous two assumptions are essentially arbitrary since their validity can only be established by certain plausibility arguments. They are utilized out of necessity to obtain approximate analytical results. Other effects, such as spanwise pressure gradients in the flow field, that introduce curvature into the slip line indicated in sketch (c), are neglected for simplicity. The errors in this

flow model will affect primarily the calculated Reynolds number in regions 10 and 11. Fortunately, the calculated heat transfer depends on the square root of the Reynolds number so the error in the theoretical heat transfer is correspondingly reduced. The Reynolds number, as well as the other properties required in regions 10 and 11 to evaluate equation (A1) are found by evaluating the change in free-stream properties through the shock-wave system shown in sketch (c).

The individual flow-field approximations used here are not an essential feature of the overall method of calculating the heat transfer associated with the impinging vortex sheet. Indeed, they are not considered to be the best approximations available. They were selected primarily because of their reasonableness and simplicity. It would be more accurate to calculate the appropriate inviscid conditions near the leading edge using measured shock-wave angles, etc., when possible before resorting to approximations such as those used here.

APPENDIX B

HEAT-TRANSFER CALCULATION

The technique described in appendix A is used to calculate leading-edge heat-transfer distributions in the neighborhood of the heating maximum for shock-generator angles of incidence between 0° and 15° for zero sweep angle. The calculation proceeds as follows: First, the strength of the impinging shock wave is determined from the shock-wave boundary-layer interaction analysis presented under Results and Discussion. With this information, the shock wave interaction pattern and the change in unit Reynolds number are found as described in appendix A. The leading-edge heat transfer is then evaluated using the average temperature in the boundary layer to find the appropriate transport properties.

As indicated in the text, the impinging shock wave appears to be the resultant of the generated shock wave and a separation-induced shock wave for shock-generator angles of incidence of 0° and 2.5°. Since the strength of the separation-induced shock wave is unknown, the strength of the resultant impinging shock wave is also unknown for these deflection angles. However, the calculated maximum heat transfer associated with the vortex impingement is only moderately dependent on the strength of the impinging shock wave (see, e.g., figs. 11(a)-11(e)), while the calculated distribution around the maximum is also a relatively weak function of the strength of this shock wave. Hence, the effects of the separation-induced shock wave are ignored when the strength of the impinging shock wave for these deflection angles is calculated. The above result, which was not known a priori, is not believed to be of general validity but is believed to be, simply, a fortuitous result for the specific cases treated here.

The results of the heat-transfer calculations near the heating maximum cannot be compared directly with experiment because the calculated heat transfer varies substantially over spanwise distances the order of a skin thickness. Thus, a thermocouple at the inner surface of the skin will not resolve the local aerodynamic heating input at the outer surface but will indicate some average rate associated with the aerodynamic heating distribution near that location. Therefore, to obtain the theoretical "indicated" value of maximum heat transfer, the thermal response of the inner surface of the model skin (where the thermocouple is physically located) to the theoretical aerodynamic heating input at the outer surface must be found. Since chordwise heating distributions are essentially constant over distances the order of several skin thicknesses, the problem reduces to the solution of the two-dimensional (spanwise and normal directions) unsteady heat conduction equation with a specified heating input at the outer surface obtained from equation (A1) of appendix A.

The two-dimensional, time dependent heat conduction equation, in difference form, was solved numerically using the procedure given by Schneider (ref. 17). First, the skin was divided into the lattice network shown in

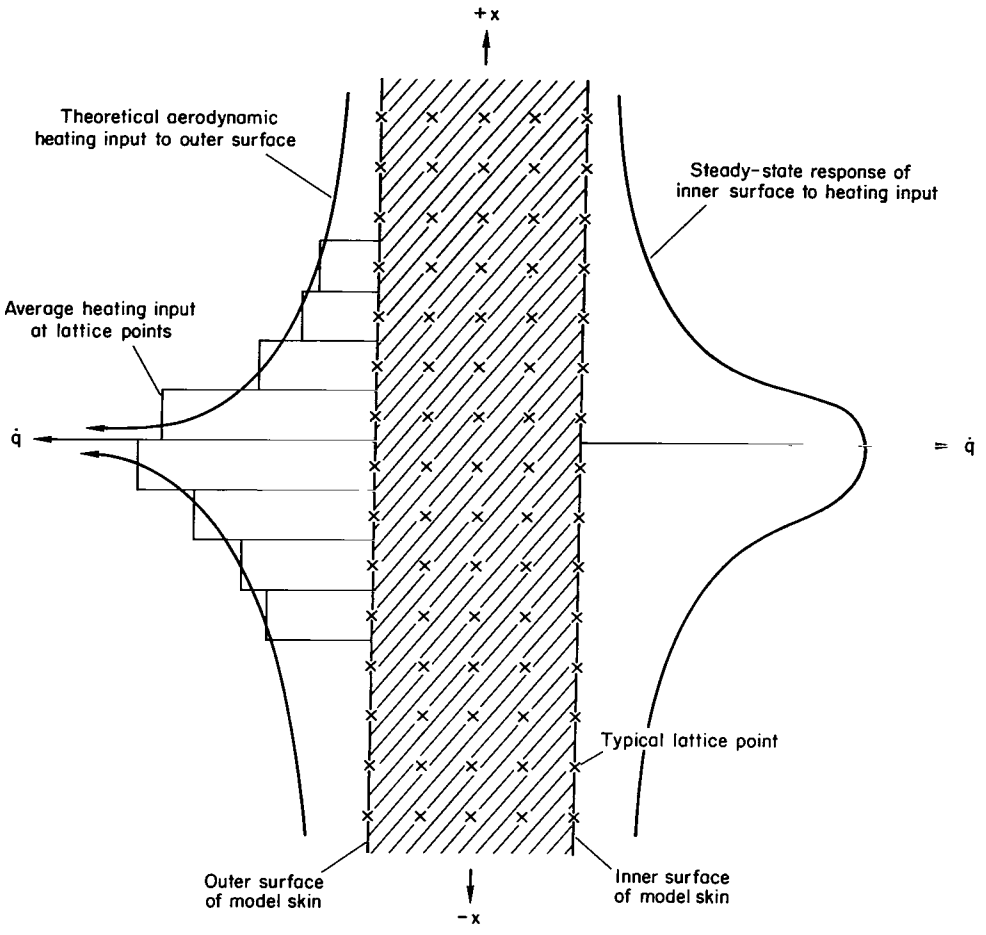

Sketch (d)

sketch (d). The heat conduction equation was then solved numerically for the rate of temperature rise at the inner surface using the appropriate average value of the heating input obtained from equation (A1) as the boundary condition for each lattice point on the outer surface by calculating the appropriate temperature rise at each lattice point shown in sketch (d). This response is averaged over the spatial extent of the thermocouple junction on the inner surface of the skin and is converted to an indicated heating rate that can be compared directly with the experimental maximum value of heat transfer. The wires that form the thermocouple junction at the location of the maximum in figure 11(b) (the only case where a thermocouple location corresponded with the location of maximum heating) are positioned side by side with a spacing of about one wire diameter. This configuration is used to determine the size of the region over which the average response of the inner surface of the skin is calculated for all cases even though a thermocouple did not exist at all locations of maximum heat transfer. The spanwise position of the theoretical maximum heat transfer is not determined by the

analysis in appendix A, but is simply assumed to coincide with the position of the experimental heat transfer maximum determined from burn markings.

The results of the preceding calculations for the heat transfer to the leading edge due to the impingement of the generated shock wave are shown in figures 11(a) through (e).

REFERENCES

1. Newlander, Robert A.: Effect of Shock Impingement on the Distribution of Heat-Transfer Coefficients on a Right Circular Cylinder at Mach Numbers of 2.65, 3.51 and 4.44. NASA TN D-642, 1961.

2. Bushnell, Dennis M.: Interference Heating on a Swept Cylinder in the Region of Its Intersection With a Wedge in Hypersonic Flow. NASA TN D-3094, 1965.

3. Beckwith, Ivan E.: Experimental Investigation of Heat Transfer and Pressures on a Swept Cylinder in the Vicinity of Its Intersection With a Wedge and Flat Plate at Mach Number 4.15 and High Reynolds Numbers. NASA TN D-2020, 1964.

4. Siler L. G.; and Deskins, H. E.: Effect of Shock Impingement on Heat-Transfer and Pressure Distributions on a Cylindrical-Leading-Edge Model at Mach Number 19. AEDC-TDR-64-228, Nov. 1964.

5. Francis, W. Leon: Experimental Heat-Transfer Study of Shock Impingement on Fins in Hypersonic Flow. J. Spacecraft Rockets, vol. 2, no. 4, July-Aug. 1965, pp. 630-632.

6. Cunningham, Bernard E.; and Kraus, Samuel: A 1-Foot Hypervelocity Shock Tunnel in Which High-Enthalpy, Real-Gas Air Flows Can Be Generated With Flow Times of About 180 Milliseconds. NASA TN D-1428, 1962.

7. Loubsky, William J.; Hiers, Robert S.; and Stewart, David A.: Performance of a Combustion Driven Shock Tunnel With Application to the Tailored-Interface Operating Conditions. Presented at Third Conference on Performance of High Temperature Systems, Pasadena, Calif., Dec. 7-9, 1964.

8. Dannenberg, Robert E.: Helium Film Cooling on a Hemisphere at a Mach Number of 10. NASA TN D-1550, 1962.

9. Hayes, Wallace D.; and Probstein, Ronald F.: Hypersonic Flow Theory. Academic Press, New York, 1959.

10. Knox, E. C.: Measurements of Shock Impingement Effects on the Heat-Transfer and Pressure Distributions on a Hemicylinder Model at Mach Number 19. AEDC-TR-65-245, Nov. 1965.

11. Halprin, Robert W.: Step Induced Boundary-Layer Separation Phenomena. AIAA J., vol. 3, no. 2, Feb. 1965, pp. 357-359.

12. Fay, J. A.; and Riddell, F. R.: Theory of Stagnation Point Heat Transfer in Dissociated Air. J. Aerospace Sci., vol. 25, no. 2, Feb. 1958, pp. 73-85, 121.

13. Ray, A. D.; and Palko, R. L.: An Investigation of the Effects of Shock Impingement on a Blunt Leading Edge. AEDC-TR-65-153, July 1965.

14. Jones, Robert A.: Heat-Transfer and Pressure Investigation of a Fin-Plate Interference Model at a Mach Number of 6. NASA TN D-2028, 1964.

15. Chung, Paul M.; and Viegas, John R.: Heat Transfer at the Reattachment Zone of Separated Laminar Boundary Layers. NASA TN D-1072, 1961.

16. Schlichting, Hermann: Boundary Layer Theory. McGraw-Hill, New York, 1955.

17. Schneider, Paul J.: Conduction Heat Transfer. Addison-Wesley Publishing Company, Inc., Cambridge, Mass., 1957.

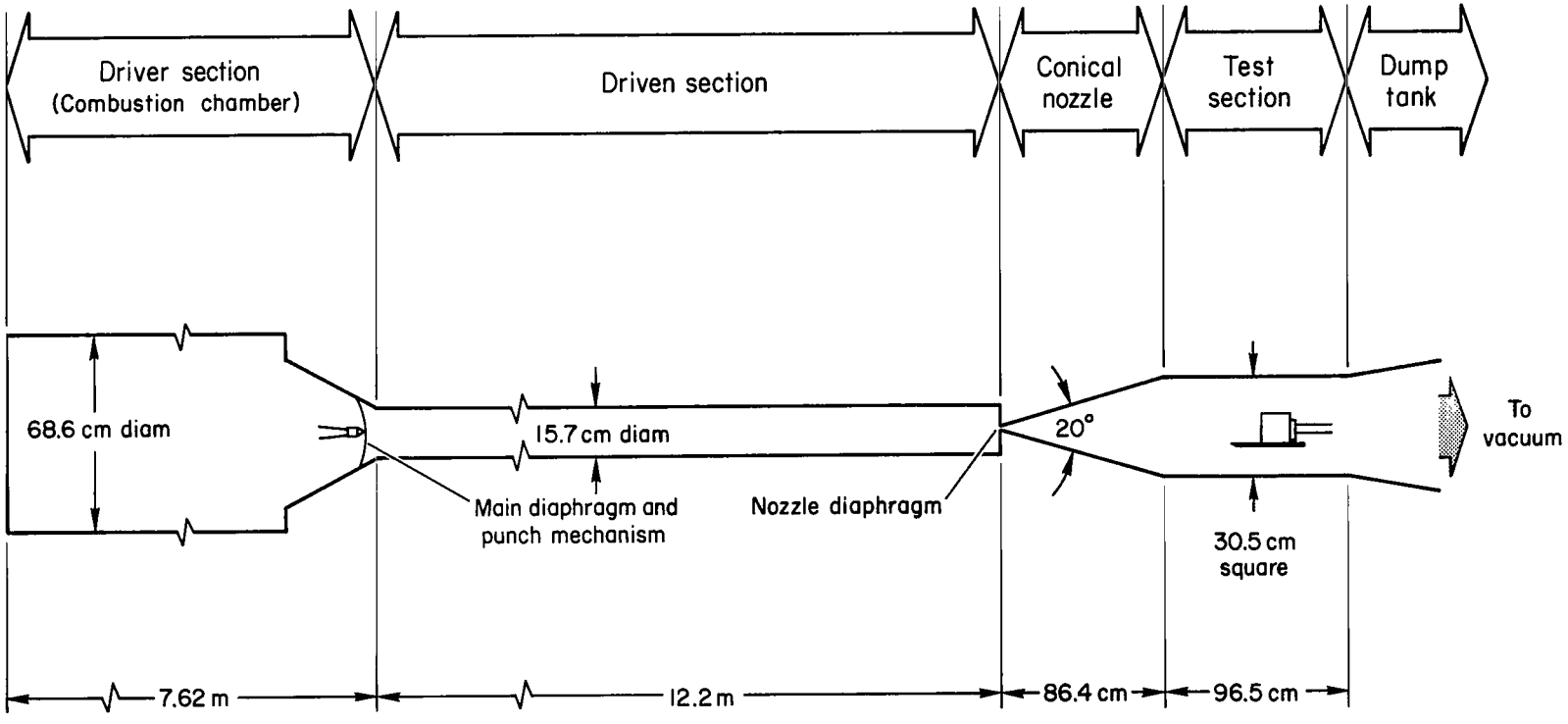

Figure 1.- Schematic drawing of the Ames 1-foot shock tunnel.

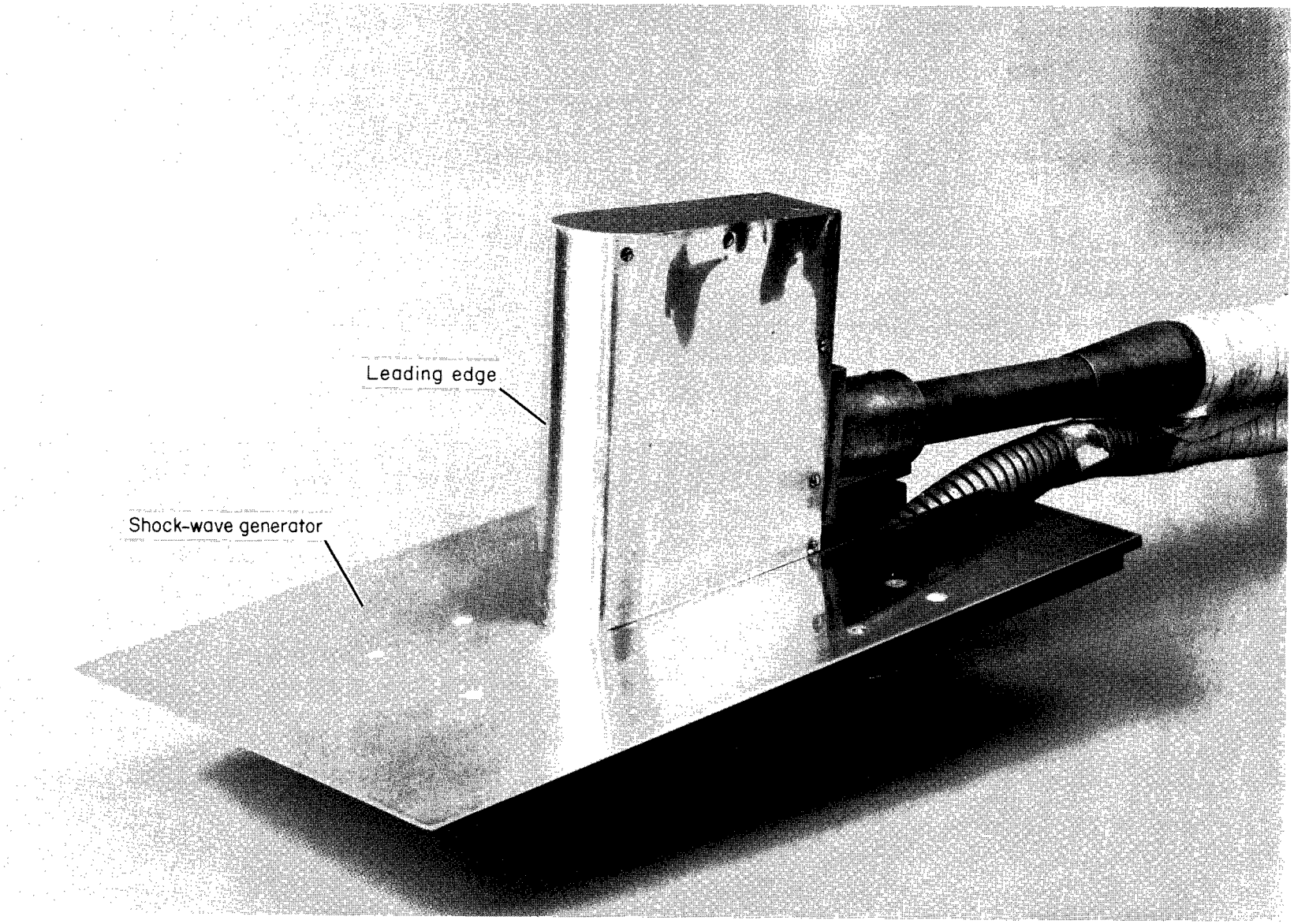

Figure 2.- Photograph of model.

A-34590.1

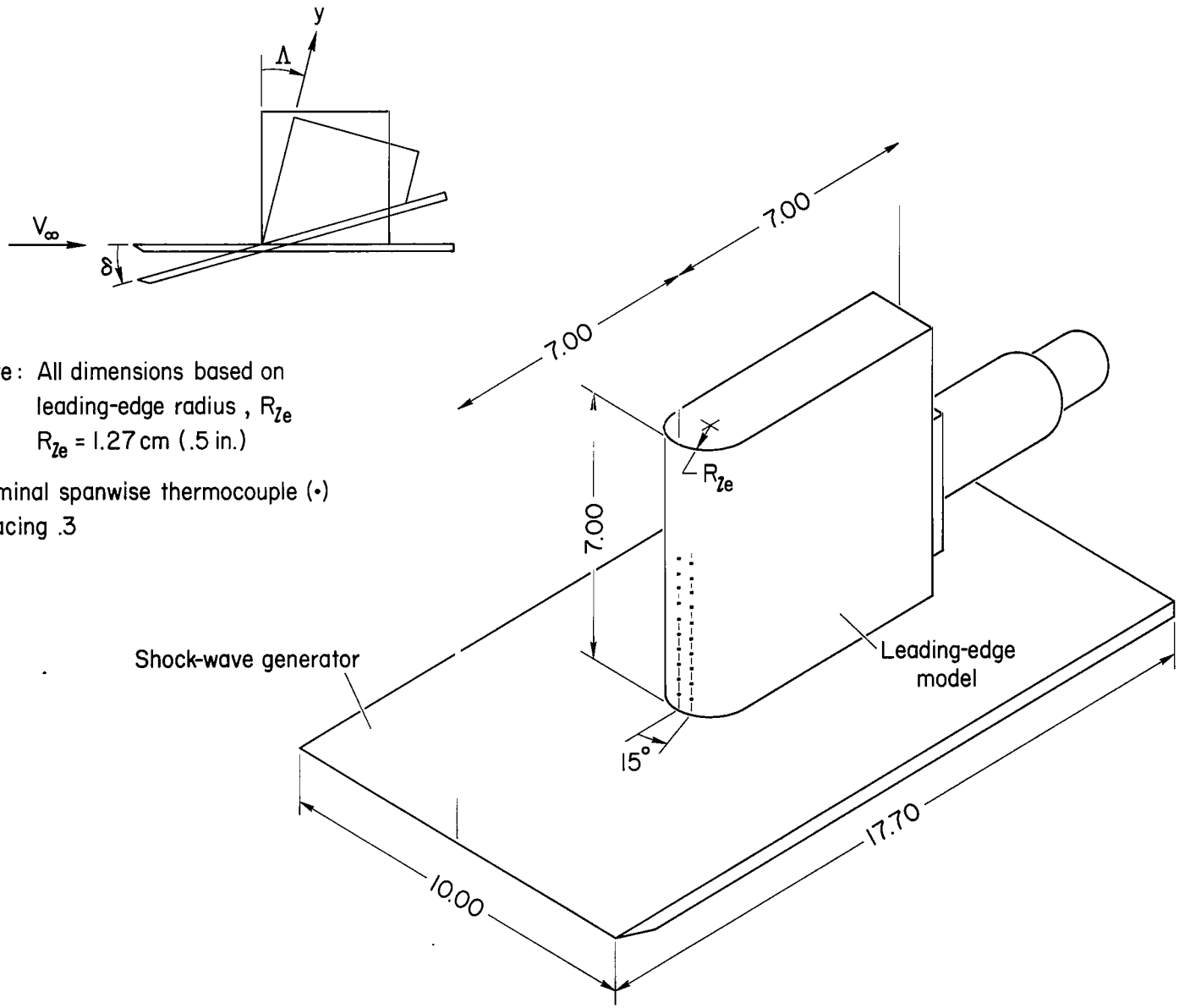

Figure 3.- Sketch of model and instrumentation.

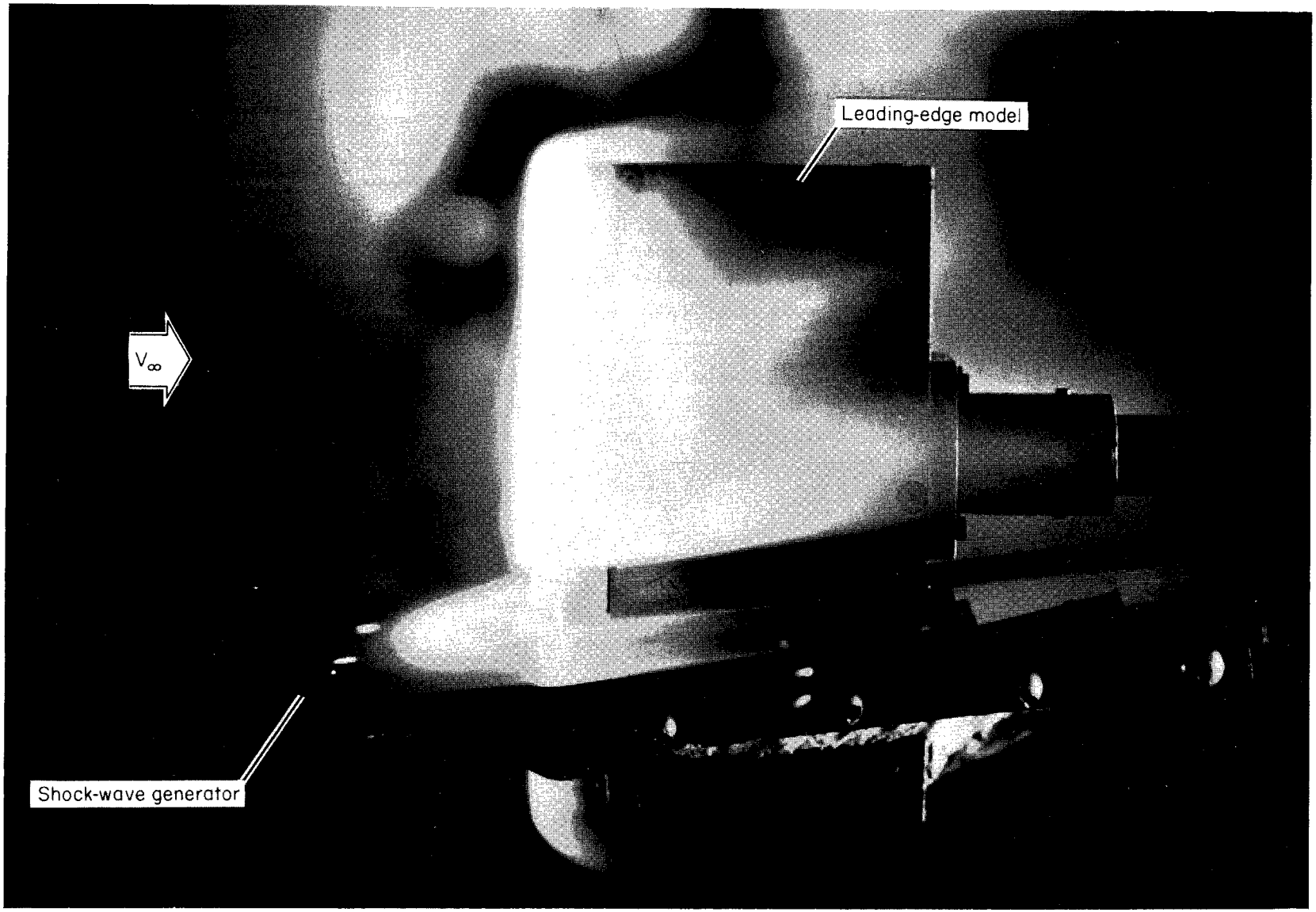

(a) Typical luminous photograph.

Figure 4.- Flow field results for $\Lambda = 0^\circ$, $\delta = 10^\circ$.

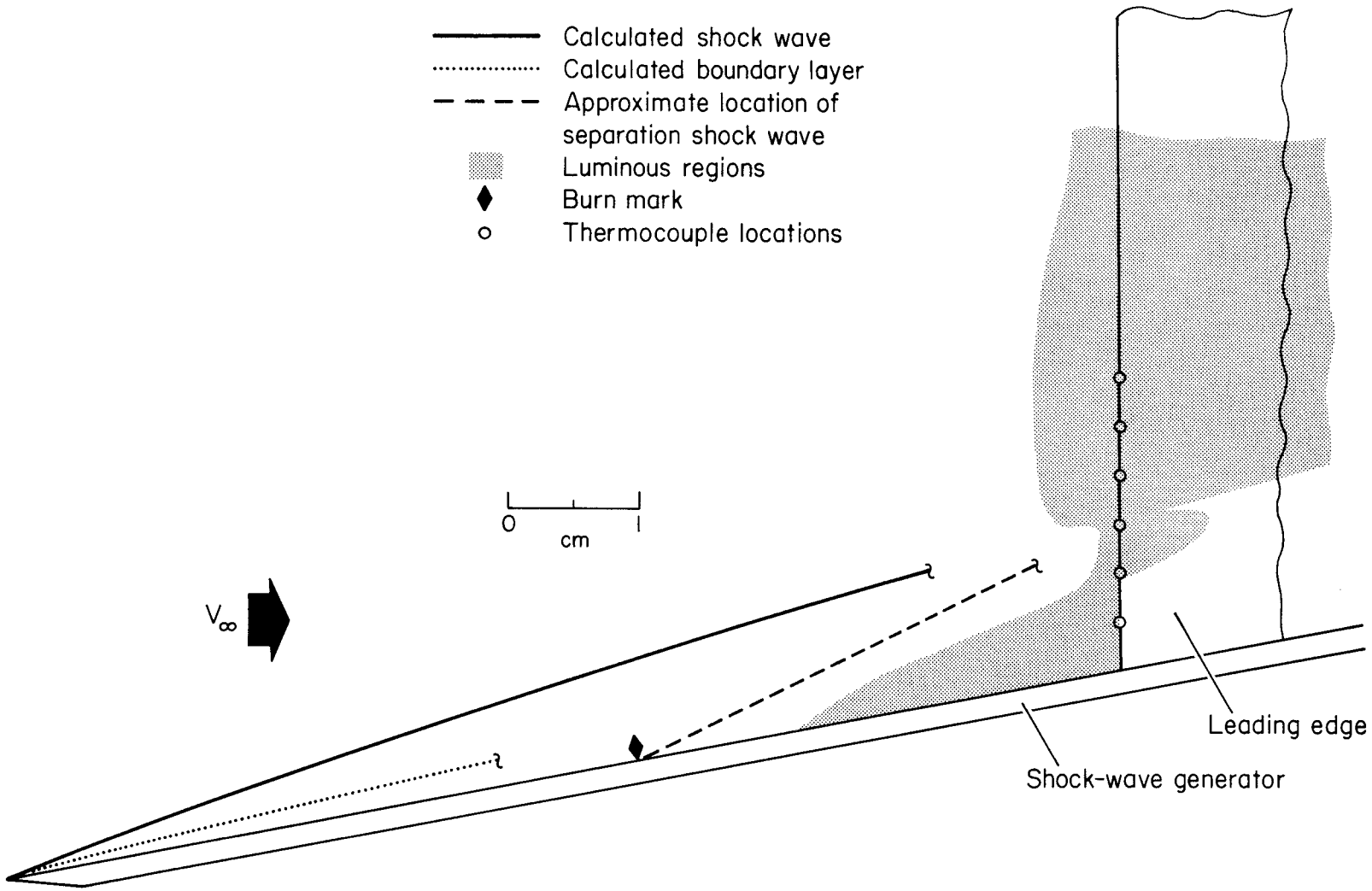

(b) Sketch of flow field.

Figure 4.- Concluded.

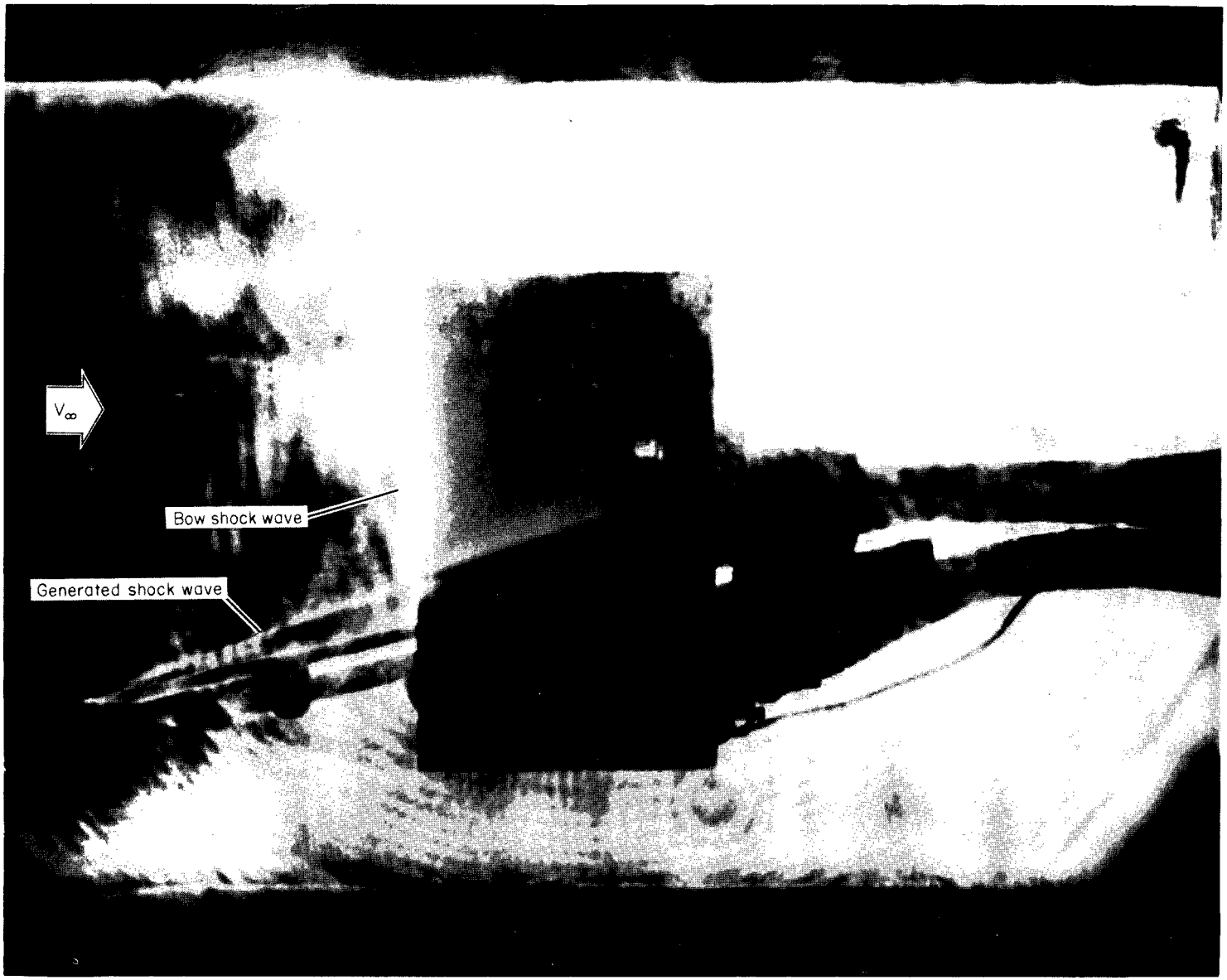

Figure 5.- Schlieren photograph, $\Lambda = 0^\circ$, $\delta = 15^\circ$.

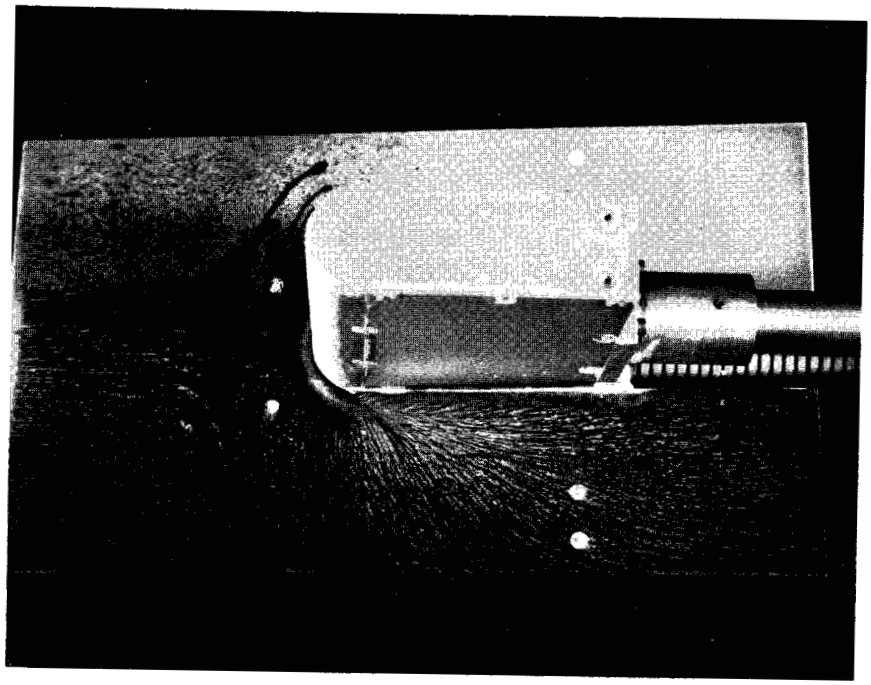

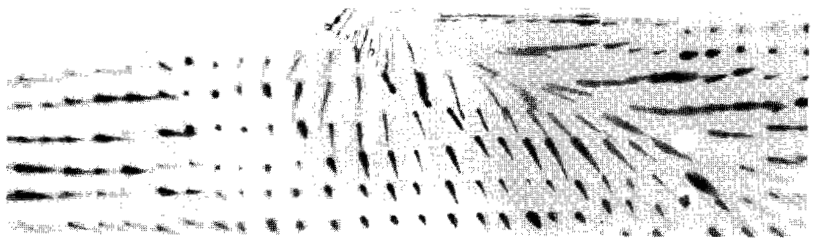

(a) Typical oil streak photographs.

Figure 6.- Shock generator oil flow results for $\Lambda = 0^{\circ}$, $\delta = 10^{\circ}$.

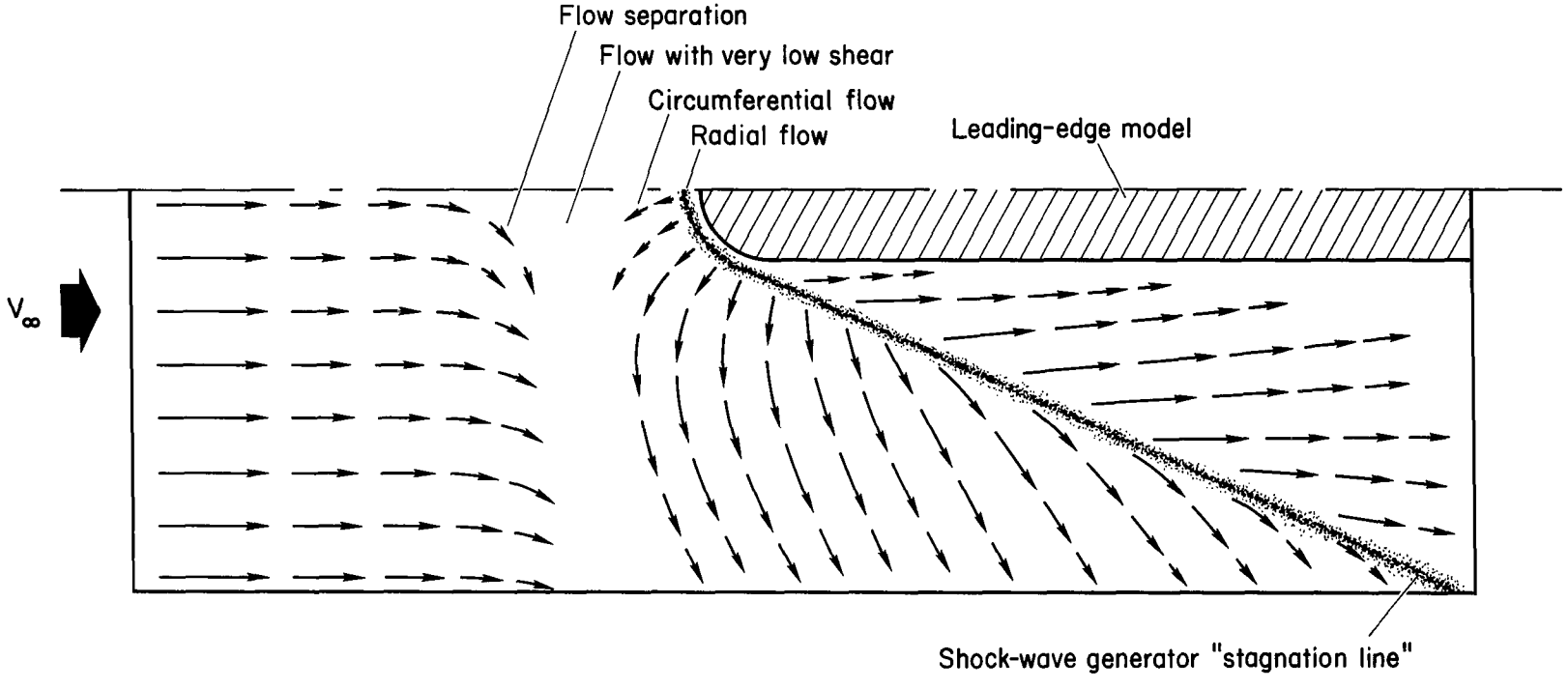

(b) Sketch of surface flow on the shock-wave generator.

Figure 6.- Concluded

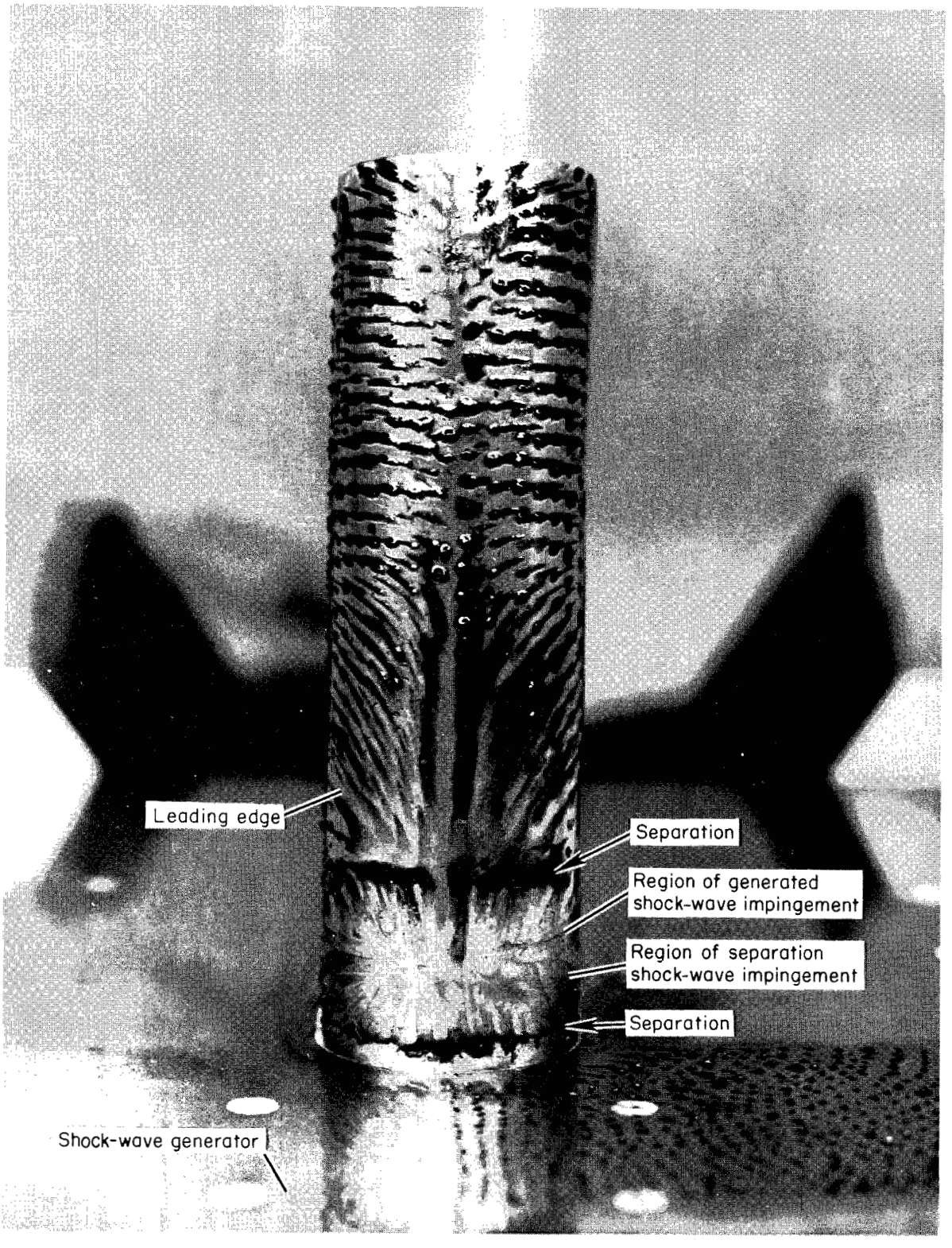

A-34977.1

Figure 7.- Leading-edge oil flow results for $\Lambda = 0^{\circ}$, $\delta = 15^{\circ}$.

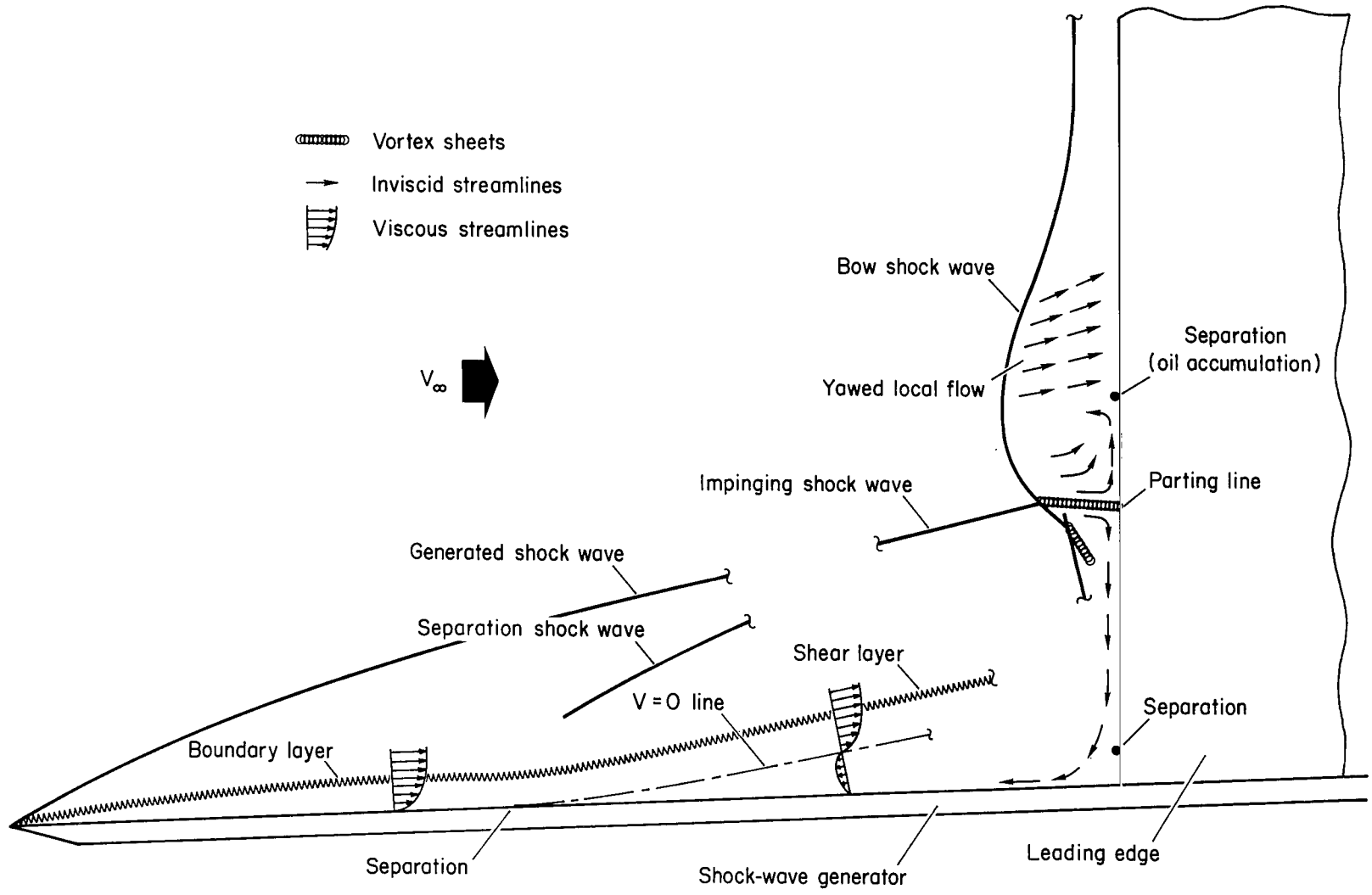

Figure 8.- Sketch of shock wave interaction and flow field for $\Lambda = 0^\circ$, $\delta = 2\text{-}1/2^\circ$.

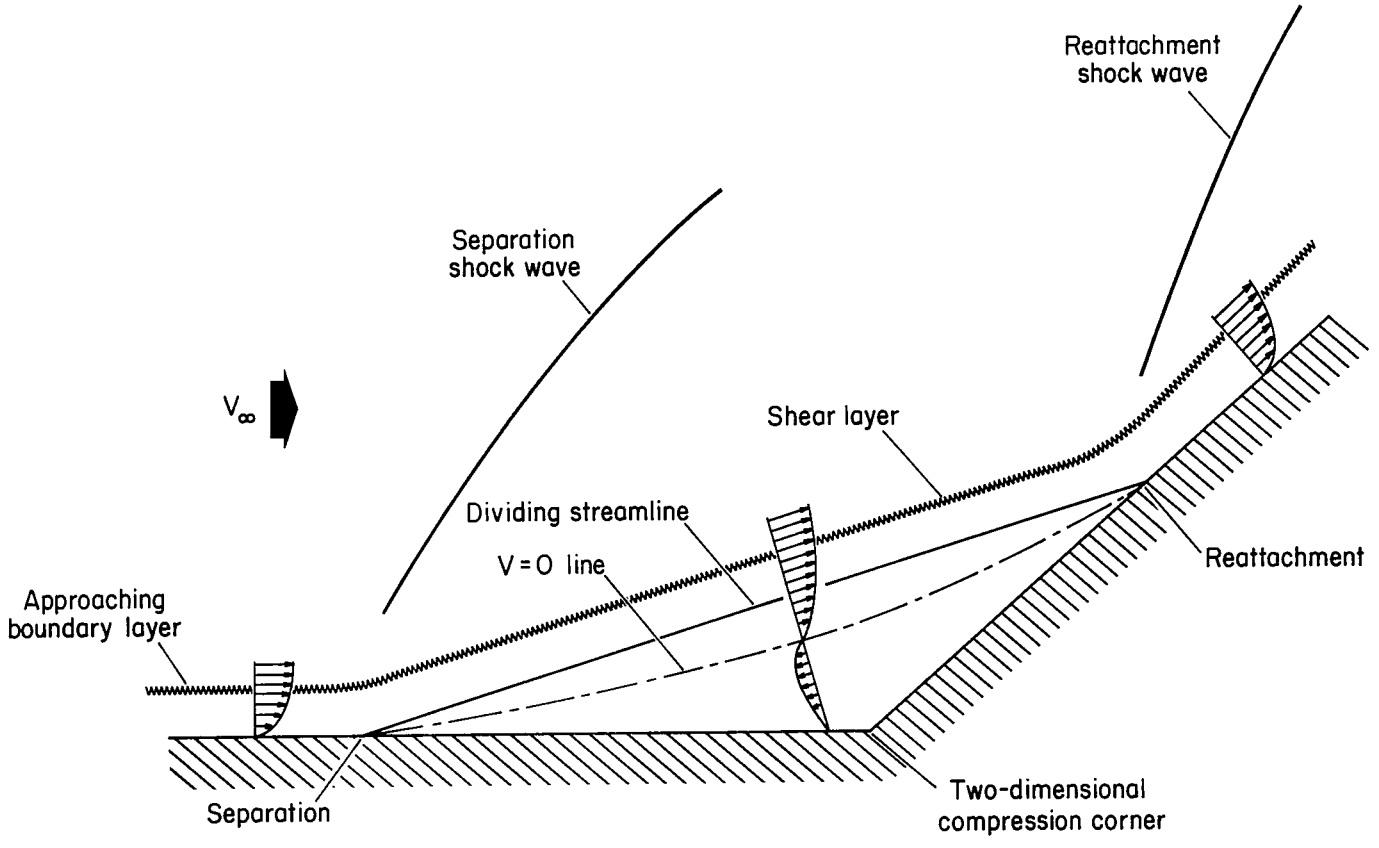

Figure 9.- Typical two-dimensional separation phenomena in the absence of shock-wave impingement.

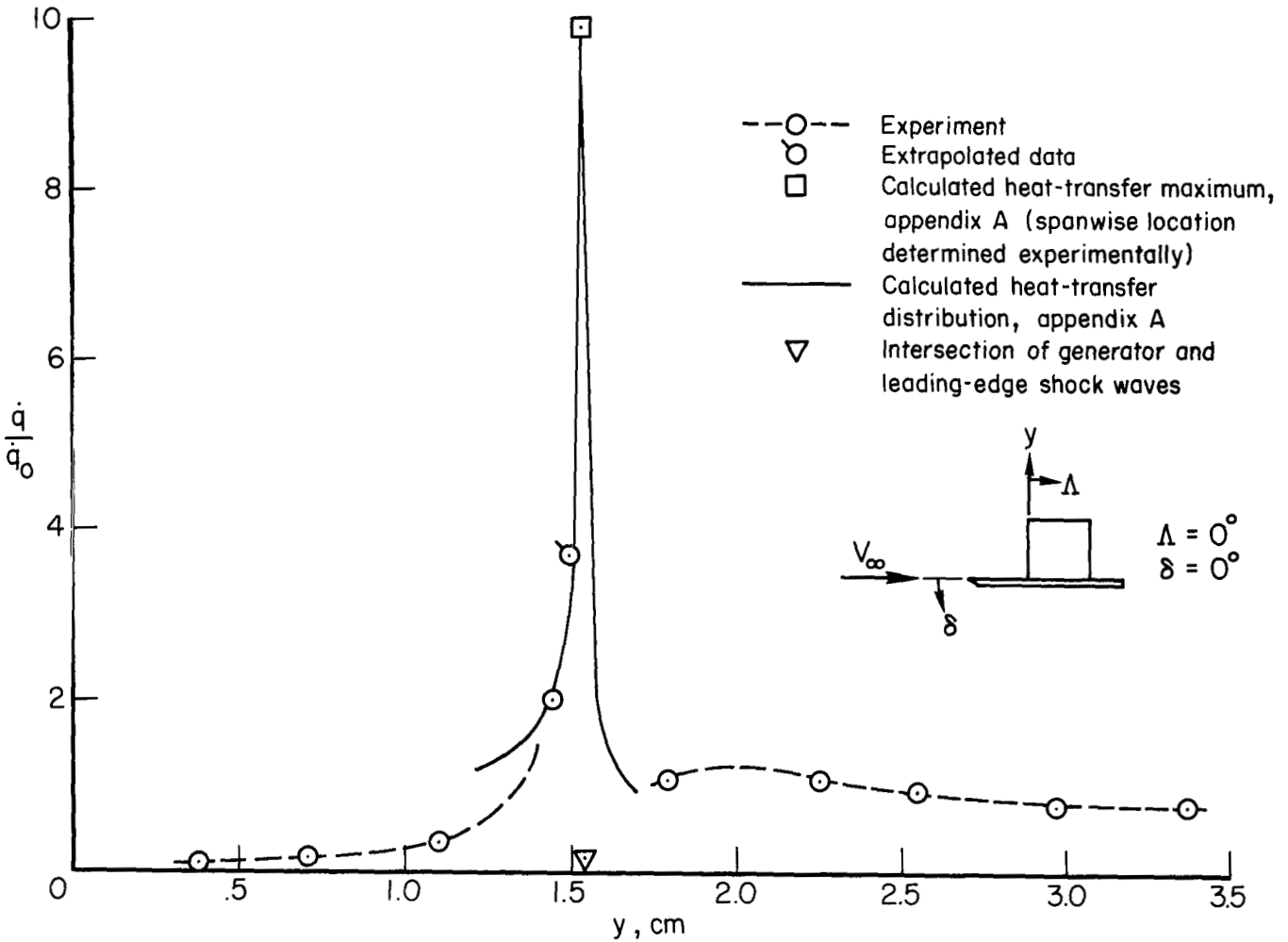

(a) $\delta = 0^\circ$

Figure 11.- Spanwise heat-transfer distributions on the stagnation line of the leading edge for $\Lambda = 0^\circ$.

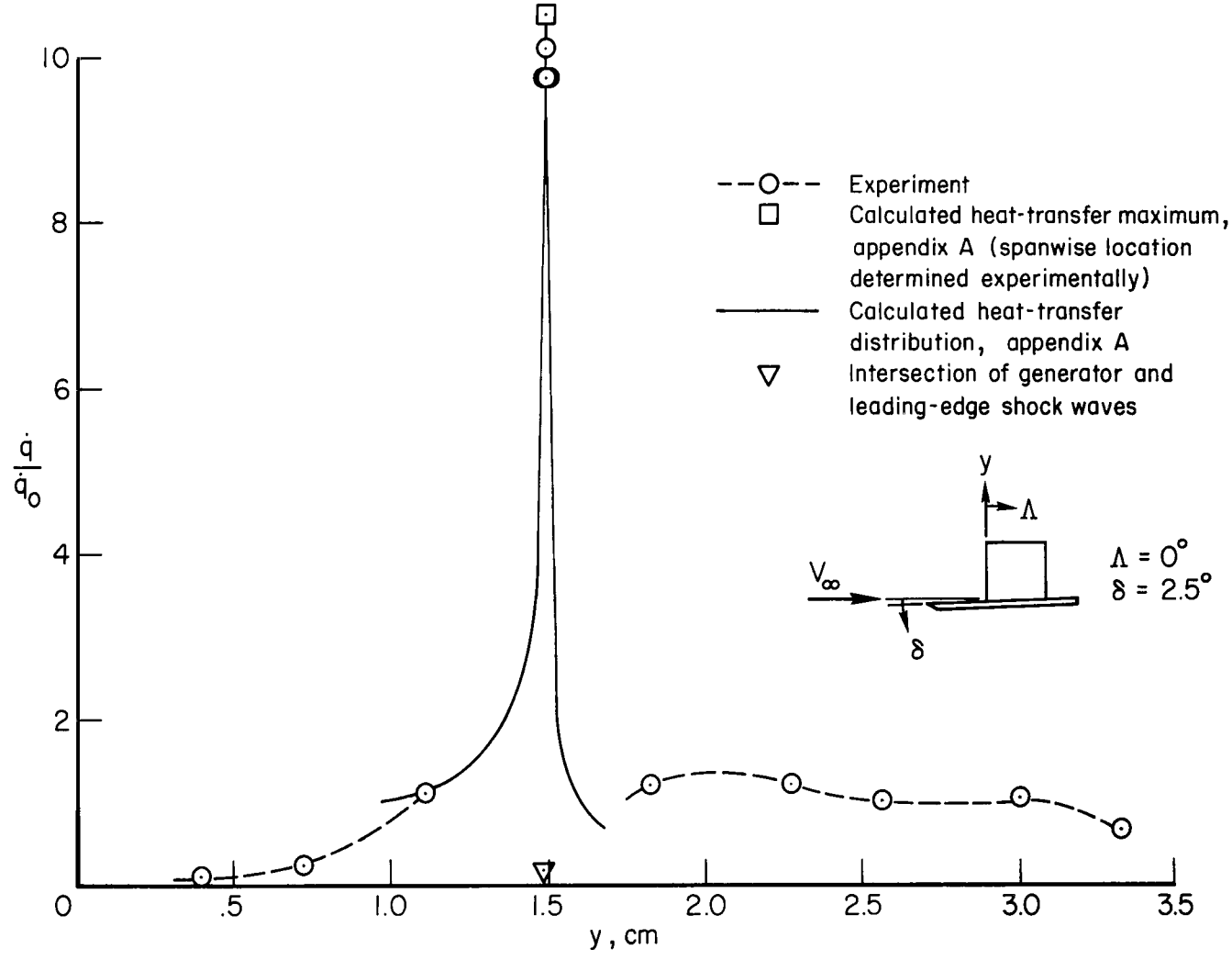

(b) $\delta = 2\text{-}1/2^\circ$

Figure 11.- Continued.

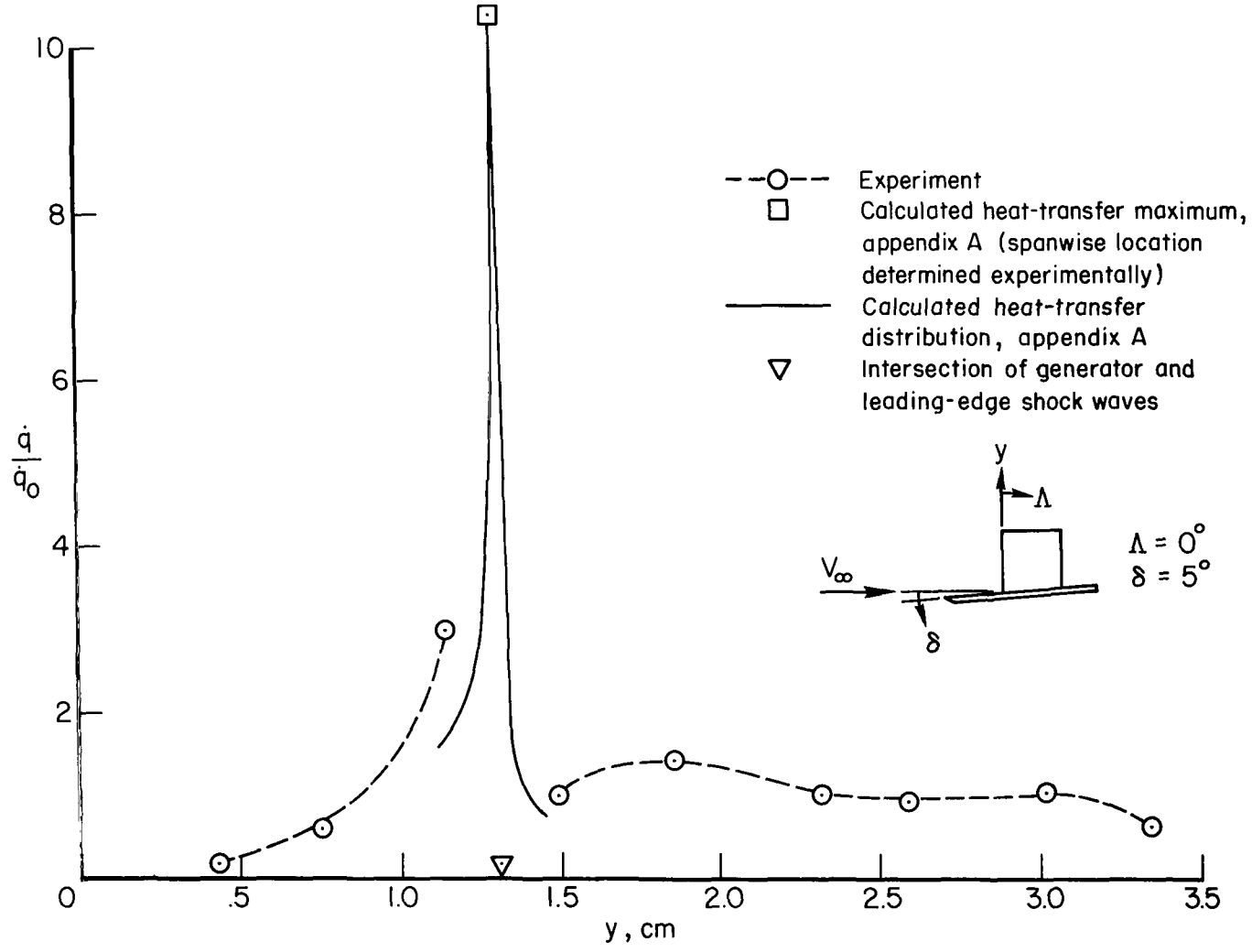

(c) $\delta = 5^\circ$

Figure 11.- Continued.

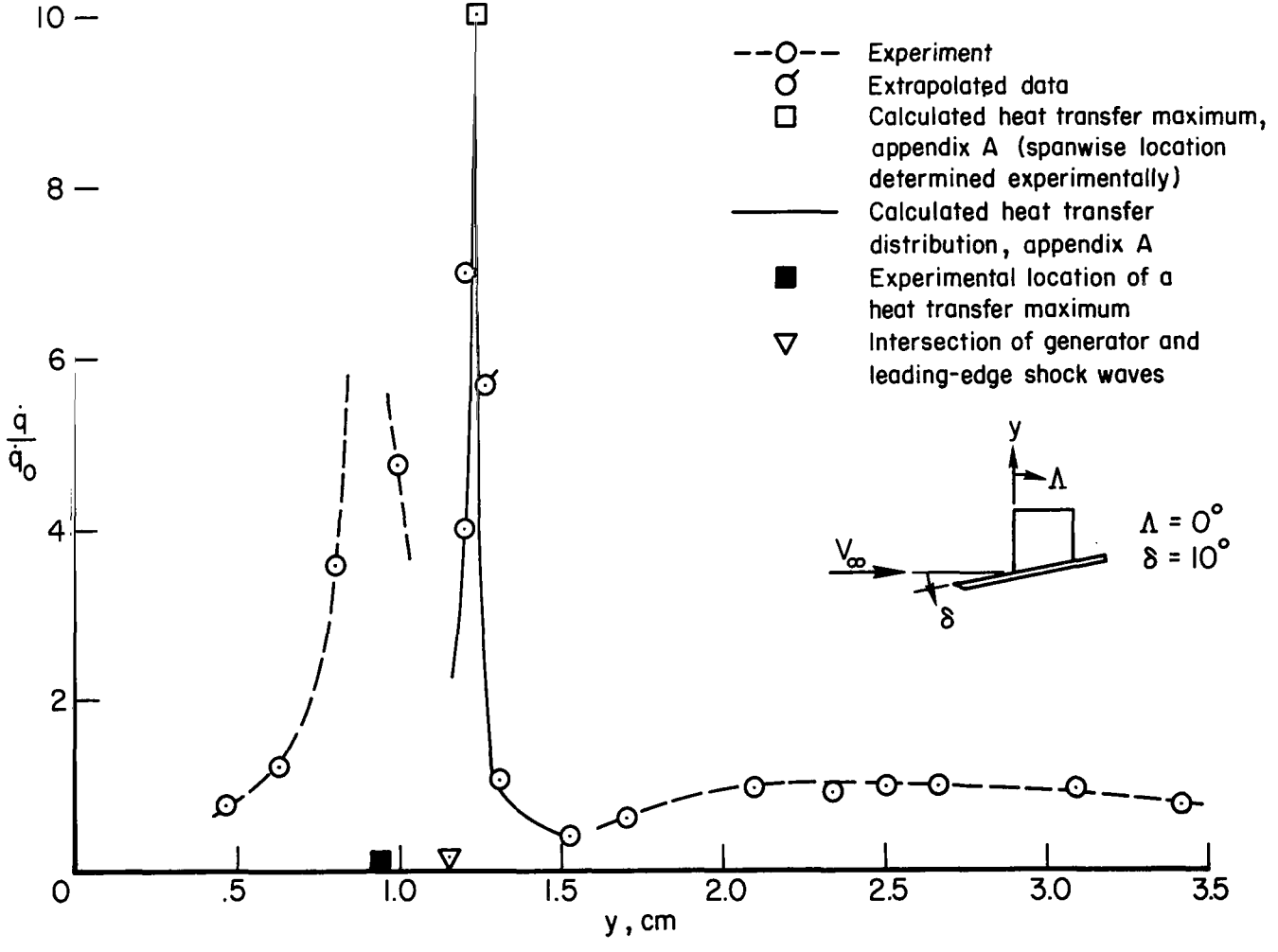

(d) $\delta = 10^\circ$

Figure 11.- Continued.

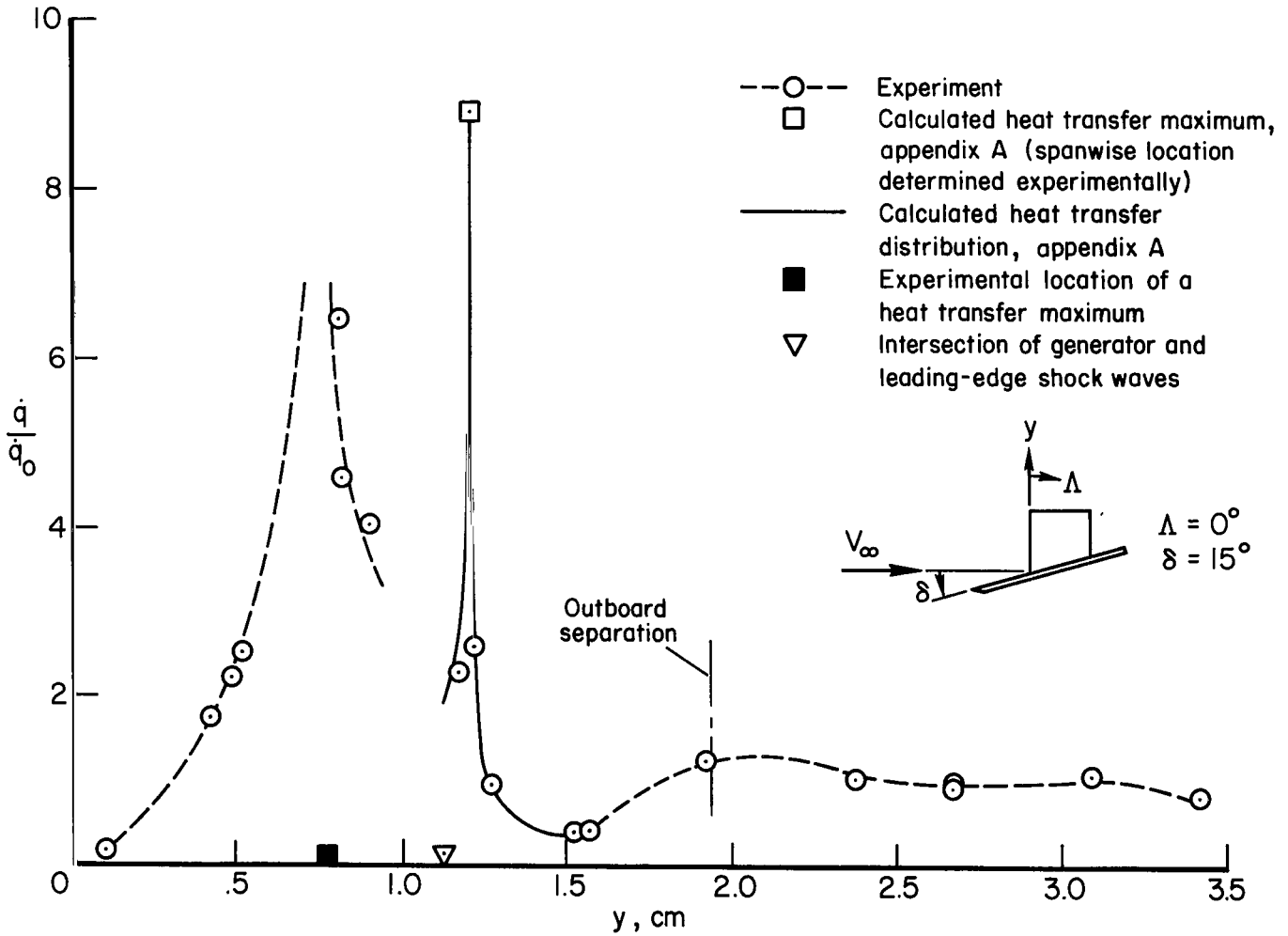

(e) $\delta = 15^\circ$

Figure 11.- Concluded.

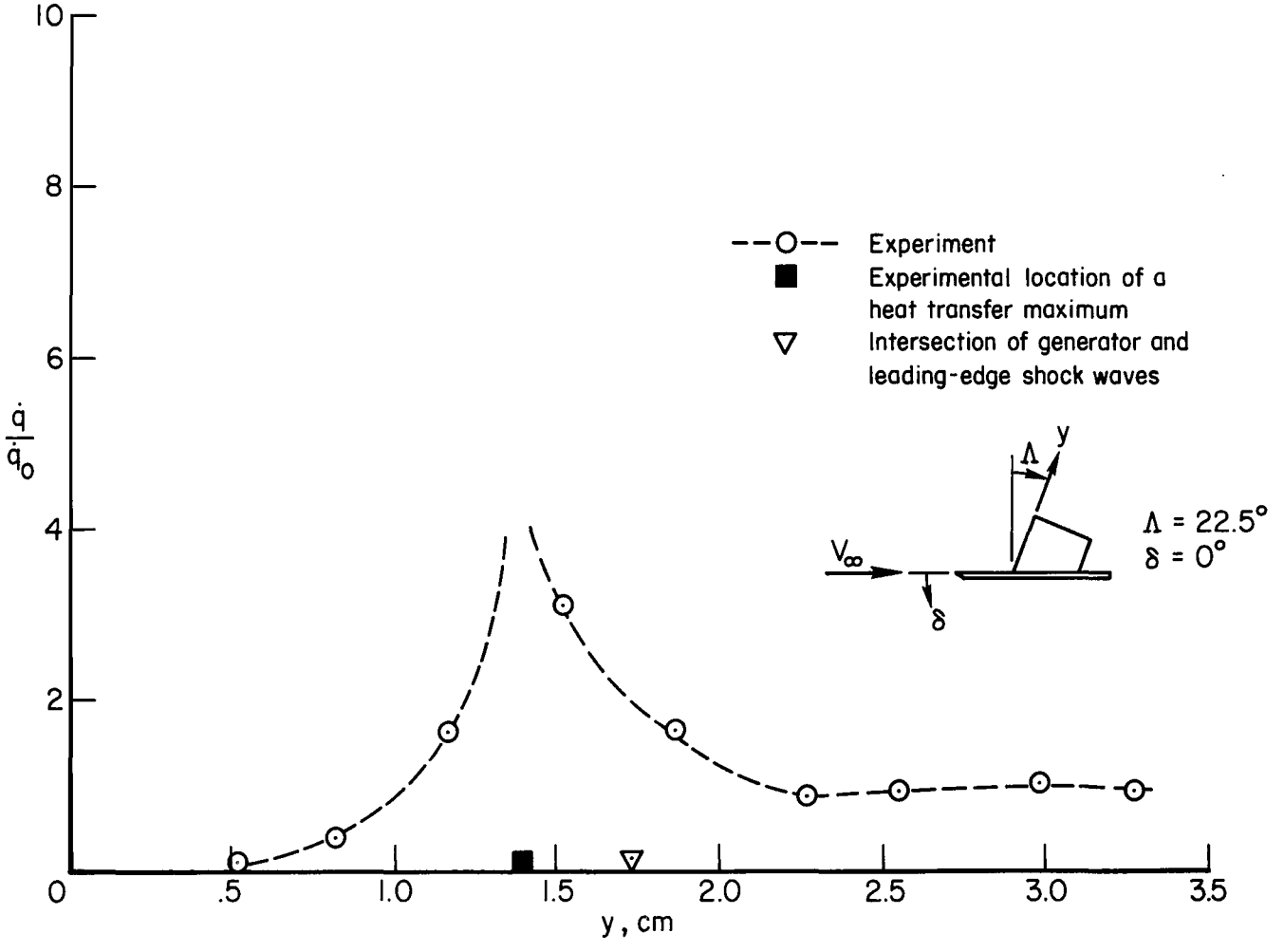

(a) $\delta = 0^\circ$

Figure 12.- Spanwise heat-transfer distributions on the stagnation line of the leading edge for $\Lambda = 22\text{-}1/2^\circ$.

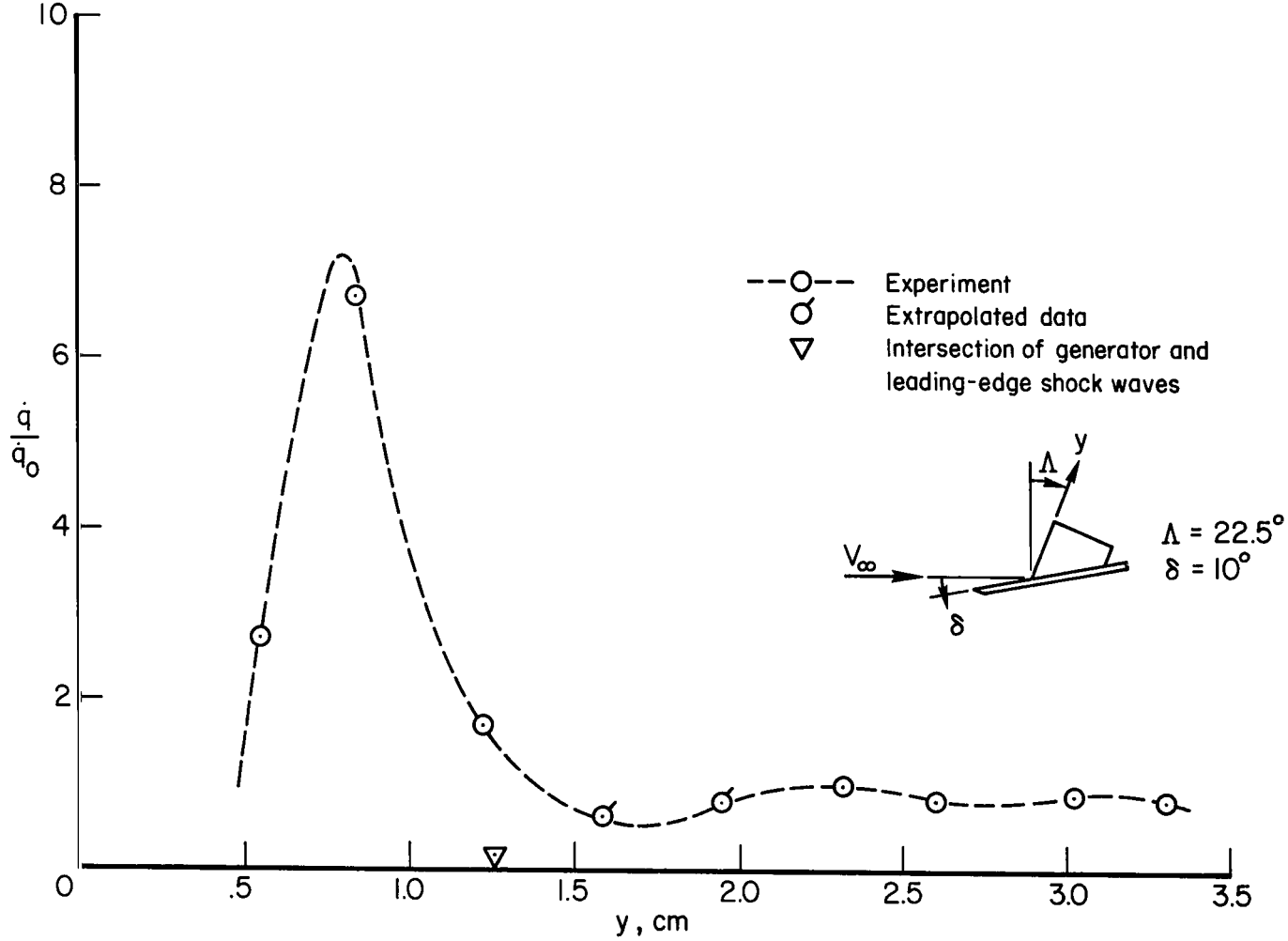

(b) $\delta = 10^\circ$

Figure 12.- Concluded.

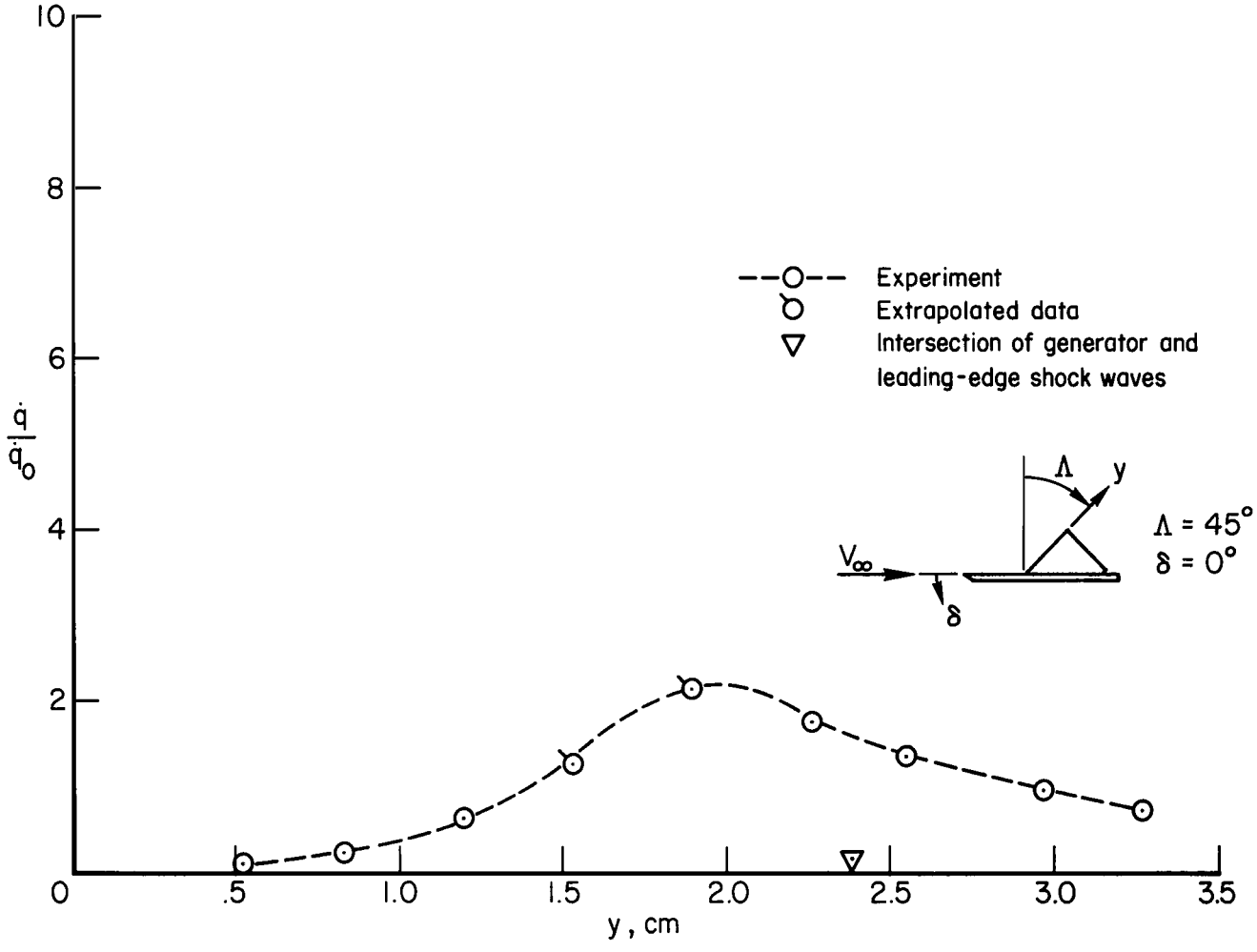

(a) $\delta = 0^\circ$

Figure 13.- Spanwise heat-transfer distributions on the stagnation line of the leading edge for $\Lambda = 45^\circ$.

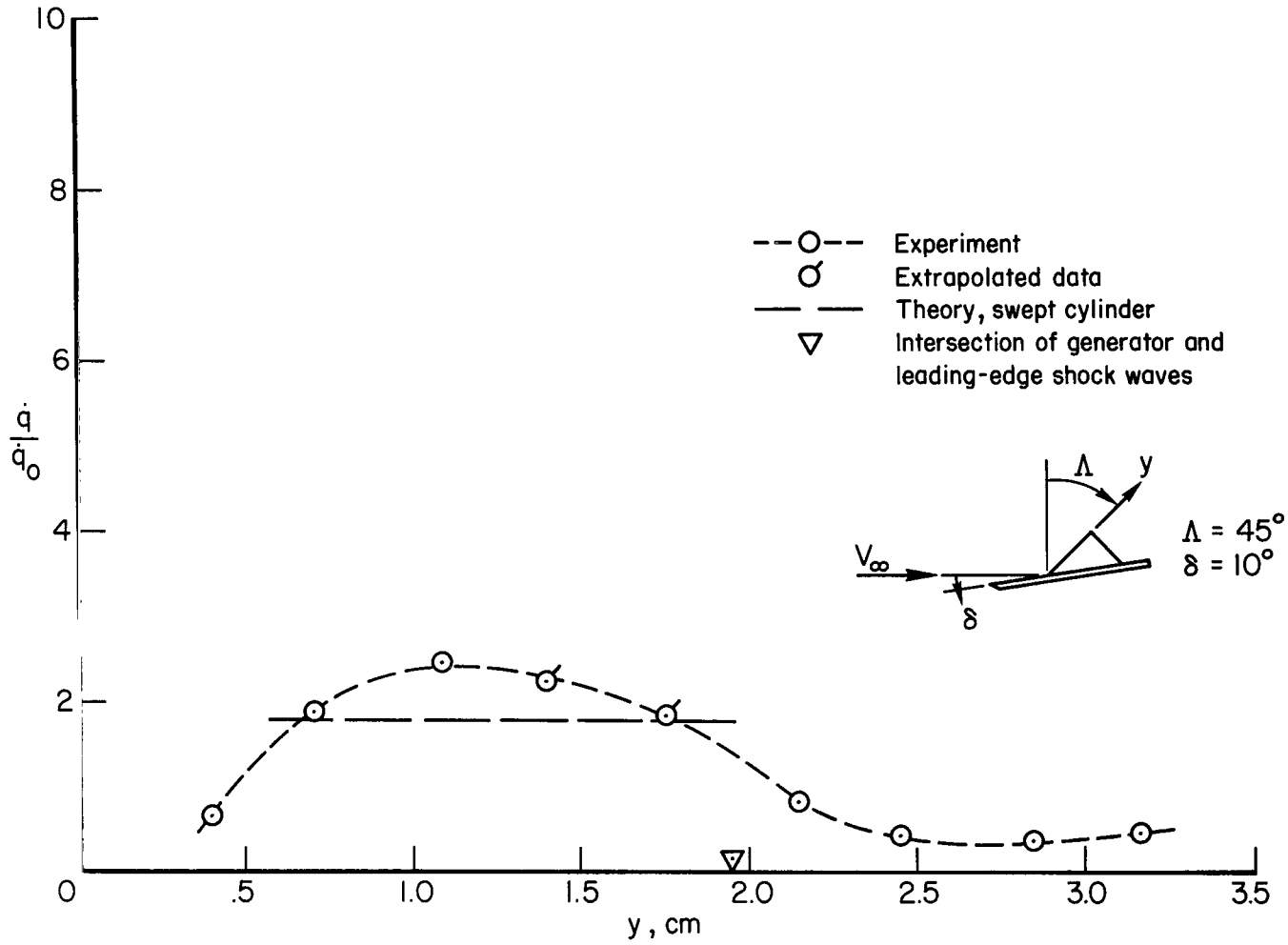

(b) $\delta = 10^\circ$

Figure 13.- Concluded.

"The aeronautical and space activities of the United States shall be conducted so as to contribute . . . to the expansion of human knowledge of phenomena in the atmosphere and space. The Administration shall provide for the widest practicable and appropriate dissemination of information concerning its activities and the results thereof."

—NATIONAL AERONAUTICS AND SPACE ACT OF 1958

NASA SCIENTIFIC AND TECHNICAL PUBLICATIONS

TECHNICAL REPORTS: Scientific and technical information considered important, complete, and a lasting contribution to existing knowledge.

TECHNICAL NOTES: Information less broad in scope but nevertheless of importance as a contribution to existing knowledge.

TECHNICAL MEMORANDUMS: Information receiving limited distribution because of preliminary data, security classification, or other reasons.

CONTRACTOR REPORTS: Technical information generated in connection with a NASA contract or grant and released under NASA auspices.

TECHNICAL TRANSLATIONS: Information published in a foreign language considered to merit NASA distribution in English.

TECHNICAL REPRINTS: Information derived from NASA activities and initially published in the form of journal articles.

SPECIAL PUBLICATIONS: Information derived from or of value to NASA activities but not necessarily reporting the results of individual NASA-programmed scientific efforts. Publications include conference proceedings, monographs, data compilations, handbooks, sourcebooks, and special bibliographies.

Details on the availability of these publications may be obtained from:

SCIENTIFIC AND TECHNICAL INFORMATION DIVISION

NATIONAL AERONAUTICS AND SPACE ADMINISTRATION

Washington, D.C. 20546